Astron. Astrophys. 174, 28–56 (1987)

ASTRONOMY
AND
ASTROPHYSICS

Hα survey of M33 with the six-meter telescope: morphology of the general diffuse emission, evidence for a chaotic medium of bubbles and filaments

G. Courtès[1,2], H. Petit[1], J.-P. Sivan[2], S. Dodonov[3] and M. Petit[1]

[1] Observatoire de Marseille, 2 Place Le Verrier, F-13248 Marseille, Cedex 04, France
[2] Laboratoire d'Astronomie Spatiale du CNRS, Traverse du Siphon, Les 3 Lucs, F-13012 Marseille, France
[3] Special Astrophysical Observatory, Nizhnij Arkhyz, Stavropolskij Kraj 357140, USSR

Received July 21, accepted October 1, 1986

Summary. A complete photographic Hα survey of M33 has been carried out with the *f*/1 focal reducer of Courtès, attached to the prime focus of the 6-m telescope of the Soviet Special Astrophysical Observatory. A list of 748 distinct H II regions has been compiled from the survey photographs. 410 nebulae are newly identified objects. The others were previously catalogued by Boulesteix et al. (1974). The photographs are presented together with identification charts. They reveal an impressive, entirely new appearance for the ionized gas in M33. The "classical" H II regions are seen bathing in a very chaotic background of Hα emission: rings, loops, arc-shaped and filamentary structures are present everywhere all over the galaxy in and between the arms.

Key words: galaxies: M33 – interstellar medium: bubbles – H II regions

1. Introduction

Hα surveys of the Milky Way by Courtès (1951a, b), Cruvellier (1967), Meaburn (1968, 1970), Georgelin and Georgelin (1970), Reynolds et al. (1974), Sivan (1974), Dubout-Crillon (1976), and Parker et al. (1979) have all revealed that Hα emission originates from bright H II regions and from the areas between the bright H II regions. Monochromatic photographs of nearby Sc and Sd galaxies (Carranza et al., 1968; Deharveng and Pellet, 1970; Monnet, 1971; Courtès, 1977) also show a diffuse background of faint, Hα emission in the arms, surrounding and connecting the discrete, bright H II regions. For some galaxies very faint diffuse Hα emission is detected over the entire disk (Monnet, 1971; Dubout et al., 1976).

Actually, from observations of the Milky Way made with a sufficiently high angular resolution (~1°), the faint Hα background does not appear as uniform emission but as filamentary and arc-shaped structures superimposed over large, diffuse areas (Sivan, 1974; Reynolds, 1980). They are typically several degree long and less than 1° wide. Obviously, to observe similar features even in the nearest galaxies, a very high angular resolution (better than, say 3″–4″) is needed. Generally this requirement is not satisfied because the detection of faint extended sources requires the use of fast focal ratios (Courtès, 1960) that unavoidably degrade the angular resolution.

One of the galaxies best suited to investigate the morphology of the ionized gas is the Triangulum galaxy, M33, due to its large angular extent (1°) and its favourable inclination, close to face-on (Maucherat et al., 1984). A complete Hα survey of this galaxy was carried out by Boulesteix et al. (1974, hereafter referred to as BCLMP) using the *f*/1 focal reducer of Courtès (1964, 1972) at the *f*/5 focus of the 1.93-m telescope of the Observatoire de Haute-Provence. The survey photographs revealed 369 distinct H II regions and confirmed the presence of the strong Hα background in the arms, noted by Carranza et al. (1968). But this background appeared to be uniform emission connecting the chains of bright, "classical" H II regions or filling the interarm, and did not show any particular structure. In a further survey, Sabbadin et al. (1980) identified numerous, small angular-diameter regions that often appear as condensations within a larger region previously catalogued by BCLMP. No information was yielded about the morphology of the Hα background.

In the Haute-Provence survey by BCLMP, the angular resolution was only limited to 3″ by the 30μm grain of the 103 aE emulsion. By adapting the same focal reducer to the prime focus of the largest telescope in the world, the 6-m telescope of the soviet Special Astrophysical Observatory in Zelentchuk, we have improved the angular resolution by a factor of 3. An almost complete Hα survey of M33 has been carried out using this new combination. It reveals a dramatic, new appearance for the interstellar matter in M33, as previously noted in some preliminary papers (Courtès et al., 1981a, b, 1982). In this paper, we present in detail all the photographs obtained to date, together with identification charts, and the new catalogue that we have compiled which contains a total of 748 H II regions.

2. Observations

The *f*/1 focal reducer was originally designed for the *f*/5 newtonian focus of the 1.93-m telescope of Haute Provence. Its adaptation to the higher focal ratio (*f*/4) beams of the prime focus of the 6-m telescope was made possible only by changing the parameters of field lens and collimator. (Note that this new combination is equivalent to a sole, *f*/1, 6-m telescope [1].) The same narrow-band

Send offprint requests to: J. P. Sivan

[1] Sixteen times more efficient than the direct *f*/4 prime focus

interference filter could be used in the focal plane of the 6-m telescope, in spite of a little change in the bandpass caused by the slight change in the beam *f*-number. The *f*/4 passband is peaked at 6552 Å and is 35 Å wide (FWHM). It should be noted that the transmission of the filter for the Hα line (whose wavelength is shifted between 6558 and 6561 Å) is always above 0.5, and then the contribution of the [N II] lines at 6548 and 6584 Å remains extremely low (<0.1 of Hα) as previously discussed (BCLMP). The 15-cm diameter of the filter limits a 20′ circular field of view. The scale is 34″.5 mm^{-1} and the angular resolution corresponding to the 30 μm pixel of the photographic emulsion is about 1″. It is most often seeing-limited and thus somewhat poorer in some photographs.

Ten long-exposure photographs have been obtained on pre-flashed Kodak 103 aE film, and developed in MWP2 developer. The relevant details of these photographs are given in Table 1. For most of them, the exposure time is of the order of 160 min; longer exposures do not improve significantly the signal-to-noise ratio for the detection of threshold signals above the background. In some cases, due to observational constraints, the photographs are a little bit less exposed, thus probably yielding a loss in contrast above the background for the faintest Hα emission features detected. As a mean, the limiting Hα surface brightness is about the same for all the survey photographs. As far as uniform, extended sources are concerned, its value must be close to that of the 1.93-m survey, since in both cases the passband of the filter, the camera *f*-number and the receptor are the same and the exposure times are of the same order. Only the spatial resolutions differ by a factor of 3. This last point leads to an higher detection when the uniform extended sources with the 193 cm telescope are, in fact, patches or filaments. This limiting surface brightness has been re-evaluated on the basis of the results of Caplan and Laval (1985) and Pellet et al. (1978). It corresponds to an emission measure of about 40 cm^{-6} pc assuming no extinction and an electronic temperature of the gas of 10^4 K.

Table 1. Observations of M 33 at the 6 meter telescope

Frame No.	Centre of the field		Exposure time (min)	Date
	R.A. 1950	DEC. 1950		
5	$1^h29^m46^s$	+30°21′42″	130	1982 Sept 22
7	1 30 04	30 36 02	120	1984 Sept 19
4	1 30 15	30 06 37	180	1982 Sept 21
3	1 30 53	30 17 37	165	1979 Sept 22
2	1 31 05	30 30 02	153	1980 Sept 9
1	1 31 14	30 47 23	162	1980 Sept 7
10	1 31 34	30 07 17	152	1984 Sept 22
6	1 31 53	30 22 38	120	1984 Sept 17
8	1 32 02	30 40 16	136	1980 Sept 19
11	1 31 02	30 24 20	180	1985 Nov 10

Notes to Table 1: All survey photographs are taken on pre-flashed Kodak 103 aE film, at *F*/1, through a 35 A FWHM Hα filter. The field diameter is 20′

3. Results

Figure 1 a is a mosaic of nine Hα photographs which gives an overall view of the survey. A chart for the identification of the nebulae is shown at the same scale in Fig. 1 b. The galaxy is almost entirely covered by the photographs, except for a small area in the south-western part of the galaxy. This missing zone results from peripheral occultations of the field, produced by the folding mirrors of the two guiding eyepieces which are mounted on the focal reducer just behind the focal plane of the telescope, and used for a fine control of the field rotation during exposures (the altazimuthal mounting of the 6-m telescope induces a rotation of the field around the optical axis).

The scale of Figs. 1 is by far too small to show all the sharp details revealed by the original films and causes a huge lost of information. This is the reason why enlargements of each photograph to a larger scale are presented in Figs. 2 a to 10 a, together with the corresponding identification charts, reproduced on the same scale in Fig. 2 b–10 b. In these figures, the original photographs of the survey are enlarged roughly 5 times. This permits to discern most (but not all) of the smallest details revealed by the original films. The numbers on the identification charts correspond to the individual H II regions catalogued in Table 2 (see below). They are drawn in different ways in order to give a very rough indication of their brightness. The brightest nebulae are fully dark, and the faintest ones are delineated by hatched contours.

Comparison of the present survey with the previous one (BCLMP) – that, as mentioned above, only differ by their angular resolutions – gives rise to a large amount of new information. This can be summarized as follows.

3.1. *Discrete* H II *regions*

The gain in spatial resolution has resulted in increasing the number of individual H II regions, with respect to the previous study. This is not surprising: as is well known, the number of nebulae detected in Hα photographs of galaxies increases when one improves the angular resolution (all other parameters being equal). Regions which were grouped together in the 1.93-m observations, are seen here separately, and faint, small-diameter regions whose dimensions were near or beneath the pixel size, become visible.

The identification of discrete H II regions in the 6-m survey was made by visual inspection of the films. It should be kept in mind that such a method is unavoidably subjective and that the number of identified nebulae depends on the "personal equation" of the observer. This well-known difficulty has been discussed in detail by Kennicutt (1979). For spatially resolved regions, ambiguity arises from their generally complex structures (bright, multiple cores) and from the absence of sharp, well-defined outer boundaries, especially in the spiral arms where the outer envelopes of the H II regions merge with the surrounding diffuse Hα background. As a general rule, we have not been trying to separate in small components nebular features that appeared, at first sight, as single, morphologically-bounded regions. Besides, this would have proved to be impossible in the case of bright regions whose images are more or less burnt out on the long-exposure photographs of the survey. For example, a single number is assigned to the NGC 604 complex, while Sabbadin et al. (1980) identified 60 distinct features within this nebula! Also, we preferred not to assign an identification number to those diffuse and/or filamentary extensions whose morphology appears rather linked to the general diffuse Hα background (see Sect. 3.3).

Table 2. Catalogue of H II regions

(1)	(2)	(3)	(4)	(5)	(6)	(7)	(8)	
				$1^h\,31^m\,12^s.1$	$30^\circ\,20'\,29''$	15x15		
1				1 31 05.1	30 22 50	9 7		
2				1 31 06.3	30 22 23	8 8	core+extension	
3				1 31 10.0	30 20 30	22 24		
4				1 31 09.1	30 20 05	16 16		
5				1 31 10.5	30 18 34	20 11		
8A				1 31 09.6	30 18 15	18 16		*
8B				1 31 02.7	30 23 32	9 9		
9				1 31 05.0	30 20 20	28 16		
10				1 31 06.5	30 19 03	20 10		
11				1 31 02.5	30 21 21	14 12	diffuse	*
12				1 31 05.0	30 17 43	24 23		*
13				1 31 01.1	30 21 45	5 5		
14				1 31 01.0	30 18 25	17 15		R
15		131		1 31 00.5	30 22 14	14 10		R
15				1 30 58.2	30 17 39	24 22	core+extension	*
17				1 30 58.7	30 18 14	8 15		
18				1 30 57.0	30 18 16	10 12		R
19				1 31 01.0	30 22 37	24 12		R
20				1 30 55.8	30 17 05	15 28		
21				1 30 55.0	30 17 50	10 12		
22				1 30 53.6	30 18 09	8 8		
23				1 30 55.6	30 21 00	12 26		
25				1 30 55.4	30 20 40	9 15		
26				1 30 55.4	30 21 33	10 8		*R
27		112		1 30 54.2	30 21 25	12 12		
28				1 30 57.9	30 23 20	12 24		
29		119		1 30 51.0	30 22 03	9 18		
30				1 30 46.1	30 21 12	15 9		
31		91		1 30 46.0	30 21 07	24 10		*
32				1 30 45.5	30 21 47	12 20		
33				1 30 43.3	30 21 35	6 8		
34		77		1 30 49.9	30 22 47	18 10		
35				1 30 49.9	30 22 38	15 10		R
35				1 30 58.3	30 23 55	10 10		
37				1 30 54.6	30 23 21	32 11	arc	R
38				1 30 52.7	30 23 35	24 10	arc	
39				1 30 54.1	30 23 43	17 28		
40				1 30 46.0	30 24 05	18 11		*R
41				1 30 44.9	30 24 14	12 10		*R
42		120		1 30 58.7	30 24 10	8 12		
43				1 30 52.5	30 24 16	7 7		
44		71		1 30 40.1	30 25 05	32 15	bright	R
45				1 30 40.6	30 25 27	12 10		
46				1 30 59.0	30 24 25	12 14		R
47				1 30 52.3	30 25 22	12 12		*R
48			N 595	1 30 44.2	30 25 20	56 104	bright core+filaments	R
49		98		1 30 50.5	30 25 44	8 8		
50				1 30 55.0	30 25 23	16 18		R
51				1 30 54.4	30 25 35	10 8		
52				1 30 50.5	30 26 15	24 18		*
53		90		1 30 46.5	30 27 12	11 8		
54				1 30 47.5	30 27 40	16 8		
55				1 30 51.9	30 25 36	12 20		
56				1 30 47.2	30 28 02	6 8		
57				1 30 50.0	30 27 44	12 8		
58				1 30 51.3	30 27 35	12 14		
59				1 30 56.6	30 27 21	18 20		
60				1 30 53.3	30 29 22	12 12	bright	
61		109		1 30 55.0	30 29 28	20 28	bright	
62				1 30 58.1	30 28 30	24 28	core+halo	R
63				1 31 00.5	30 26 15	16 28		
64				1 31 03.2	30 28 32	16 16		
65				1 31 02.7	30 25 35	16 18		
66				1 31 00.6	30 24 36	15 15		
69				1 31 01.2	30 24 48	21 12		
70				1 31 01.2	30 24 54	21 12		
71				1 31 11.5	30 28 37	8 11		
72		155		1 31 08.2	30 22 47	12 18		
73				1 31 08.8	30 27 10	12 12		
74		144		1 31 07.0	30 25 55	6 6		
75				1 31 07.0	30 25 39	8 8		
76				1 31 17.0	30 25 30	22 28	bright	
77				1 31 21.5	30 27 16	14 10		
78				1 31 11.0	30 25 30	19 13		
79		153		1 31 11.5	30 25 03	10 8		*
80				1 31 11.8	30 24 42	18 16		
81				1 31 20.2	30 23 52	18 18		R
83				1 31 07.8	30 23 57	6 6		
84				1 31 17.8	30 24 06	12 20		
85				1 31 06.9	30 23 38	13 13		
86				1 31 12.9	30 23 25	26 40	bright	
87				1 31 26.3	30 21 52	34 26	bright	R
88				1 31 11.5	30 22 55	36 26	bubble	
89A				1 31 13.0	30 22 23	10 16	core+diffuse extension	
89B				1 31 14.5	30 22 46	7 7		R
90				1 31 17.0	30 22 30	14 14		R
91				1 31 06.0	30 23 34	11 7	diffuse	
92				1 31 02.9	30 23 55	24 28	bright	
93				1 31 11.0	30 22 48	14 16		
94				1 31 21.7	30 20 58	14 24	core+halo	
95				1 31 21.6	30 20 30	8 12		
95A				1 31 07.4	30 23 05	15 20		
96				1 31 12.0	30 22 02	8 16	core+halo	*
97				1 31 04.0	30 23 32	18 20	bright	
99				1 31 12.0	30 21 00	64 32	bright core+loop	
100				1 30 50.1	30 17 15	15 20		
200	101			1 30 51.6	30 16 45	16 24		
201				1 30 49.7	30 16 45	10 10		R
202				1 30 48.2	30 16 38	6 6		R
203								

(1)	(2)	(3)	(4)	(5)	(6)	(7)	(8)	
				$1^h\,30^m\,50^s.0$	$30^\circ\,16'\,10''$	24 36		R
204				1 30 48.5	30 14 48	11 12		
206				1 30 46.0	30 14 32	12 10	core+halo	*
207				1 30 44.8	30 15 45	32 19	multicore	
208		81		1 30 43.8	30 18 25	5 28	core+extension	
209		74		1 30 42.0	30 18 14	8 8		*
210				1 30 41.0	30 16 26	11 7		
211				1 30 40.0	30 16 37	7 9		
212				1 30 38.5	30 16 30	16 20	core+extension	
213				1 30 40.8	30 16 24	16 13		
214				1 30 25.5	30 17 13	18 14		
215				1 30 22.0	30 14 28	12 32	core+extension	R
216				1 30 19.5	30 14 35	36 24	bright	
217				1 30 11.2	30 15 25	40 44	bright core+halo	*R
218	219	30		1 30 22.0	30 12 15	19 17	bright	
220		45		1 30 20.7	30 12 05	16 24	bright	
221		42		1 30 35.5	30 10 10	16 28		
222			I 135	1 30 35.5	30 15 30	17 14		
223				1 30 31.5	30 16 43	20 20	core+extension	
224				1 30 32.0	30 16 10	8 14		
225				1 30 23.0	30 15 08	5 12	core+halo	
226				1 30 22.5	30 14 53	12 13		
227				1 30 12.8	30 19 25	18 19		
229				1 30 11.5	30 18 54	40 26	core+halo	
230				1 30 10.5	30 19 24	14 10		R
231				1 30 08.6	30 19 23	9 16		
232				1 30 08.5	30 20 40	33 6	arc	R
233				1 30 07.0	30 20 17	18 5		
234				1 30 06.2	30 20 30	5 14		
235				1 30 03.0	30 20 22	22 22		
236				1 30 03.8	30 19 35	14 28	core+extension	R
237				1 29 55.5	30 19 33	10 16		
238				1 30 08.0	30 17 33	7 9		R
239				1 30 07.0	30 17 06	11 12		
240		27		1 30 08.1	30 16 40	7 11		
241				1 30 07.0	30 12 10	15 22		
243				1 30 29.8	30 11 45	50 36	bubble	
245				1 30 52.0	30 07 18	15 26	core+arc	
246				1 30 54.0	30 07 10	16 20		R
247				1 30 56.3	30 06 17	14 12		
248		111		1 30 50.9	30 05 28	28 16		R
249				1 30 48.5	30 05 24	60 16	core+extension	
250				1 30 46.0	30 04 50	32 14	core+extension	
251		92		1 30 41.5	30 03 17	8 8	starlike	
252				1 30 40.3	30 02 35	10 20	core+extension	
253		72		1 30 32.0	30 02 33	9 14		
254				1 30 21.0	30 07 45	28 16		
255				1 30 22.5	30 08 05	31 32	bright	R
256				1 30 20.5	30 08 06	10 11		
257		41		1 30 17.0	30 08 10	14 24		
258				1 30 18.0	30 07 38	14 21		
259				1 30 05.7	30 07 58	24 34	core+halo	R
261				1 29 56.8	30 05 05	24 20	core+halo	
262		21		1 29 53.5	30 05 45	24 32	bubble+diffuse extension	
263				1 29 51.8	30 07 08	16 16	core+extension	R
264				1 29 54.8	30 08 45	25 7	arc	
265				1 29 51.5	30 09 05	10 32	core+extension	
266		11		1 29 53.0	30 09 45	32 32		
268				1 29 52.3	30 09 55	24 10		R
269				1 29 57.6	30 09 43	11 19		R
270				1 29 45.0	30 12 20	18 24	bubble	
272				1 29 43.2	30 15 06	15 15	missed by 6m survey	
273				1 29 43.0	30 19 55	80 48	core+bubble	R
274		5		1 29 40.9	30 20 45	7 16	core+extension	
275			N 592	1 30 22.0	30 23 30	17 14	core+extension	
277				1 30 29.8	30 24 14	12 8		
278				1 30 06.9	30 24 08	12 5		
279			N 588	1 29 56.5	30 23 40	36 26	bright	
280				1 29 49.0	30 24 35	36 46	bubble	R
281				1 29 54.1	30 25 07	5 7	diffuse	
282				1 30 07.1	30 25 15	24 28		
283				1 30 14.8	30 24 30	10 10		*
284				1 30 17.5	30 25 43	8 8		
285				1 30 25.5	30 26 17	12 12		*
286				1 30 29.0	30 25 58	8 12		*
287				1 30 18.0	30 27 18	40 24	core+extension	
288				1 30 09.2	30 29 05	6 8		
289				1 31 06.2	30 30 10	36 24	bright	R
301		138	I 142	1 31 17.5	30 32 12	38 20	bright	
302		167		1 30 25.5	30 30 34	12 12		
601				1 30 28.0	30 30 25	20 16		
602				1 30 27.5	30 31 25	20 16		
603				1 30 27.5	30 31 23	7 5		
604				1 30 31.0	30 32 33	32 32	bubble	
605				1 30 32.4	30 32 29	12 36		
607				1 30 36.4	30 32 28	40 44	bubble	
608				1 30 40.0	30 32 29	44 32		
609				1 30 44.5	30 31 47	10 16		
610				1 30 44.8	30 32 20	28 14		
611				1 30 51.3	30 30 35	12 32		
612		104		1 30 53.0	30 32 29	5 12		
613				1 30 54.7	30 33 18	5 6		
614				1 30 45.3	30 33 24	44 8	arc	
615				1 30 05.2	30 35 06	8 8		
616				1 30 24.3	30 35 15	18 8		
618				1 30 25.5	30 35 48	4 4		
619				1 30 25.5	30 36 18	9 9		
620		51		1 30 24.7	30 36 55	8 15		
621				1 30 26.2	30 36 50	5 5		
622				1 30 27.0	30 37 30	48 24	core+extension	
623		56	I 133					

Table 2 (continued)

(1)	(2)	(3)	(4)	(5)	(6)	(7)	(8)	
624				$1^h30^m26^s.0$	30°38'02"	32 28	core+halo	
625				1 30 25.8	30 38 12	17 17		
626				1 30 27.0	30 38 40	23 36	core+extension	
627				1 30 34.9	30 35 10	8 10		
628				1 30 45.0	30 34 50	8 8		
629				1 30 47.0	30 35 17	12 16		
630				1 30 45.6	30 35 27	24 20	diffuse	
631				1 30 58.2	30 35 34	20 20		
632				1 31 00.0	30 35 20	36 40	core+halo	R
633		114		1 31 57.0	30 36 55	6 8		
634				1 30 52.3	30 37 15	56 20	diffuse halo	
635				1 30 54.0	30 37 48	16 9	diffuse halo	
636				1 30 58.0	30 38 40	8 10		
637		127		1 31 01.0	30 41 15	48 36	bright core+halo	
638		55	I 132	1 30 26.5	30 41 25	36 48	strong	
639				1 30 38.6	30 45 00	8 32	core+diffuse halo	
640				1 30 45.2	30 45 35	60 80	bubble	
641				1 30 55.0	30 46 55	68 56	core+bubble	R
643				1 31 23.0	30 53 55	72 72	bubble	R
644				1 31 38.8	30 50 50	8 8		
645				1 31 19.5	30 48 00	12 12		
646A				1 31 16.8	30 48 12	12 20		
646B				1 31 24.0	30 49 20	76 40	diffuse	
647				1 31 20.9	30 46 45	68 12	arc	
648				1 31 17.0	30 45 42	36 40		
649				1 31 49.0	30 47 07	24 28	core+halo	
650				1 31 43.2	30 45 07	48 60	bubble	R
651		200		1 31 39.8	30 41 55	32 28		
652				1 31 42.0	30 41 25	32 28	halo	
653				1 31 48.8	30 40 53	16 9	filament	
654				1 31 50.6	30 40 50	16 3		
655				1 31 52.4	30 40 24	10 7	diffuse	
656				1 31 56.4	30 40 07	15 15		
657				1 32 00.0	30 39 35	28 40	core+halo	
659				1 31 34.3	30 41 45	14 14		
660				1 31 24.5	30 40 05	76 80	diffuse bubble	R
661		196		1 31 31.8	30 39 05	7 7	starlike	
662				1 31 34.5	30 39 35	11 11		
663				1 31 36.5	30 38 25	68 64	diffuse bubble	R
664				1 31 38.0	30 37 32	48 36	diffuse bubble	R
665				1 31 24.4	30 38 15	16 56	diffuse	
666				1 31 26.5	30 37 20	36 36	diffuse bubble	R
667				1 31 23.5	30 37 00	36 6	arc	R
668				1 31 14.3	30 39 35	20 16		
669		147		1 31 09.5	30 40 10	8 8		
670		162		1 31 13.6	30 37 46	7 7	starlike	
671				1 31 17.0	30 36 22	16 7		
672		161		1 31 13.5	30 35 14	24 20	core+halo	
673				1 31 12.0	30 35 50	10 14		
674				1 31 09.0	30 35 58	20 12	diffuse	
675				1 31 12.9	30 35 10	8 8		
676				1 31 42.5	30 33 45	15 12		
677				1 31 51.4	30 32 59	24 20	core+halo	
678				1 31 51.7	30 31 47	6 6		
679		213		1 31 47.6	30 31 56	7 7	starlike	
680		211	N 604	1 31 43.4	30 31 45	72 116	bright+extension	*R
681				1 31 47.1	30 31 18	10 11		
682				1 31 33.5	30 31 32	10 16	diffuse	
683				1 31 33.7	30 33 34	11 20	knot+diffuse extension	R
684				1 31 32.0	30 33 20	40 16		R
685				1 31 30.5	30 33 40	22 24		
686				1 31 28.3	30 33 23	18 10		
687				1 31 24.4	30 33 10	16 32	core+extension	R
688				1 31 21.8	30 31 18	16 12		R
689				1 31 19.0	30 31 25	24 12		
690				1 31 17.8	30 31 43	8 12		
691		189		1 31 27.0	30 36 31	26 28	bright	R
692				1 31 14.0	30 32 45	18 20		
693				1 31 14.5	30 31 41	20 16	core+halo	
694		130		1 31 02.5	30 31 58	8 8		
695		146		1 31 09.4	30 33 53	7 7		
696				1 31 08.7	30 33 18	20 20		
697				1 31 03.0	30 31 14	8 8		
698				1 31 12.0	30 29 43	9 7		
699				1 31 11.0	30 29 19	6 6	starlike	
702				1 31 20.8	30 16 35	21 16	core+extension	
703		151		1 31 10.5	30 17 22	8 8		
704				1 31 07.0	30 16 46	56 8	arc	
705				1 31 51.0	30 16 03	10 7		
706		218		1 31 53.0	30 16 25	12 16	knot+diffuse extension	
707				1 31 06.2	30 18 34	9 40		
708				1 31 18.7	30 18 44	9 8		
709				1 31 21.8	30 19 20	36 40	ring	
710		177		1 31 24.5	30 18 25	16 13		R
711				1 31 28.1	30 18 22	16 40	core+halo	R
712		194		1 31 30.0	30 18 25	18 16		*R
713				1 31 29.1	30 19 15	14 13		
714		176		1 31 26.0	30 19 24	44 36		R
715				1 31 33.5	30 17 56	30 12	core+arc	
716				1 31 33.0	30 17 20	5 5		
717				1 31 45.0	30 20 04	12 15		
718				1 31 46.0	30 20 33	20 20	core+halo	
719				1 31 43.0	30 20 51	12 9		
720				1 31 27.0	30 21 25	12 12		
721				1 31 31.8	30 22 43	12 6		
722				1 31 29.2	30 23 18	6 6	starlike	
723		188		1 31 27.2	30 24 02	6 6		
724				1 31 30.1	30 24 00	28 6	arc	
725				1 31 57.5	30 22 52	11 16	core+halo	
726		222		1 31 57.9	30 22 37	4 4	starlike	

(1)	(2)	(3)	(4)	(5)	(6)	(7)	(8)	
729				$1^h31^m49^s.5$	30°22'41"	19 19	diffuse bubble	*
730				1 31 47.8	30 22 53	6 8	diffuse	
731				1 31 35.5	30 24 28	9 9		
732				1 31 23.7	30 24 45	16 8		
733				1 31 23.5	30 24 57	8 10		
734				1 31 40.9	30 25 15	11 20		R
735				1 31 41.0	30 25 00	11 8	core+halo	
736				1 31 44.5	30 25 44	3 5		
737				1 31 48.8	30 25 35	10 10		
738		216		1 31 49.7	30 25 47	12 11		
739				1 31 52.3	30 25 55	8 18		
740		217		1 31 50.3	30 26 30	20 32	bright	R
741				1 31 47.7	30 26 25	8 8	diffuse	
742				1 31 49.5	30 26 02	12 8		
743				1 31 25.5	30 27 06	60 28		
744				1 31 24.0	30 26 41	9 9		
745		214		1 31 48.0	30 19 39	14 11	core+halo	
746				1 31 31.0	30 29 06	24 24	diffuse ring	
747				1 31 23.2	30 29 48	10 10		
748				1 31 47.1	30 28 50	10 16		
749				1 31 49.5	30 28 45	18 28		R
750				1 31 51.0	30 28 15	32 32	core+halo	*
751				1 31 17.6	30 21 12	28 20	diffuse bubble	
752				1 32 05.5	30 26 00	20 22		
753				1 32 09.8	30 26 15	12 8	diffuse	
754				1 32 10.5	30 20 48	20 24	diffuse	
755				1 32 17.7	30 26 25	13 28		
758				1 31 07.5	30 12 00	32 18		R
1001				1 30 56.8	30 20 43	12 15		
1002				1 30 54.5	30 20 10	16 20		
1003				1 30 49.4	30 19 42	12 10		
1004				1 30 47.5	30 20 24	13 20	core+extension	
1005				1 30 44.5	30 22 07	20 20	core+halo	
1006				1 30 42.0	30 22 46	26 16		
1007				1 30 37.0	30 23 45	20 24	bright	R
1008				1 30 46.9	30 23 27	8 10		
1501				1 31 03.5	30 17 10	8 6		
1502				1 30 55.2	30 16 26	24 38		
Z	1			1 29 53.6	30 05 02	8 8		
Z	1A		154	1 31 10.0	30 19 19	32 52	bright core+extension	R
Z	2			1 29 53.3	30 06 47	13 13	ring	
Z	2A			1 31 02.9	30 18 08	12 12	diffuse ring	
Z	3	257		1 29 49.0	30 09 35	10 24	core+extension	
Z	3A	257		1 29 50.8	30 09 38	10 12		
Z	3B	257		1 29 51.7	30 09 32	9 7		
Z	4			1 29 46.3	30 10 04	4 4	diffuse	
Z	4A			1 31 07.8	30 19 50	11 8		
Z	5			1 29 45.8	30 11 02	4 6	diffuse	
Z	6	271		1 29 45.0	30 11 42	9 8		
Z	7	271	7	1 29 45.8	30 11 50	10 12	core+halo	
Z	8			1 29 55.5	30 06 55	7 7	diffuse	
Z	9			1 29 56.3	30 07 57	9 9	diffuse	
Z	10	24		1 30 53.1	30 17 52	12 12		
Z	10A	24		1 30 53.0	30 17 37	14 14		
Z	11			1 29 58.0	30 06 28	9 9	diffuse	
Z	12			1 30 05.0	30 02 55	6 6	diffuse	
Z	13			1 30 05.0	30 10 20	11 12	core+halo	
Z	14			1 31 05.2	30 21 29	7 4		R
Z	15			1 30 06.0	30 08 23	4 7		
Z	16			1 30 07.5	30 08 27	10 36	diffuse	
Z	17			1 30 07.9	30 08 00	18 13	diffuse	
Z	18	260		1 30 10.2	30 09 00	9 7		
Z	19			1 30 10.5	30 08 22	12 8	diffuse	R
Z	20			1 30 07.0	30 10 33	14 12		
Z	21	260		1 30 11.0	30 09 17	5 6		
Z	22	260	31	1 30 12.3	30 09 15	13 8		
Z	23			1 30 24.5	30 14 24	9 9		
Z	23A			1 30 14.3	30 08 03	20 20		R
Z	24			1 30 14.2	30 07 05	9 9	diffuse	
Z	25			1 30 13.3	30 14 15	8 8		R
Z	26			1 30 14.5	30 14 28	4 4		
Z	26A			1 30 17.8	30 14 50	50 35		
Z	27			1 30 14.8	30 13 35	10 12	core+halo	
Z	27A			1 30 16.4	30 13 53	44 56	bubble	
Z	28			1 30 19.5	30 12 33	16 10		
Z	29		43	1 30 21.6	30 02 47	6 6	starlike	
Z	30			1 30 23.3	30 07 40	6 6	starlike	
Z	30A			1 30 26.0	30 08 30	5 40	filamentary	R
Z	31			1 30 23.5	30 12 50	8 15	core+extension	
Z	32			1 30 24.2	30 07 22	4 4	starlike	
Z	33			1 30 48.0	30 17 45	15 15		
Z	33A			1 30 48.1	30 18.20	24 44	diffuse	
Z	34		50	1 30 25.0	30 11 47	8 10		R
Z	35			1 30 30.4	30 03 03	8 10		
Z	36			1 30 31.0	30 11 15	6 6		
Z	37			1 30 32.7	30 10 40	10 10		
Z	38			1 30 32.6	30 10 23	5 4		
Z	39			1 30 34.9	30 03 28	7 7	diffuse	
Z	40			1 30 33.3	30 11 42	5 5		
Z	41			1 30 34.3	30 11 12	7 6		
Z	42			1 30 34.7	30 10 54	6 8		
Z	43			1 30 37.0	30 08 47	10 10		
Z	43A			1 30 33.0	30 10 58	68 44	bubble	
Z	44		73	1 30 41.6	30 03 13	5 5	starlike	
Z	45			1 30 41.2	30 03 34	12 12	diffuse	
Z	46			1 30 39.8	30 01 46	6 6		
Z	47			1 30 43.2	30 04 55	6 6	starlike	
Z	48			1 30 44.0	30 05 10	7 7	starlike	
Z	49			1 30 45.0	30 04 35	5 5	starlike	
Z	50			1 30 46.5	30 09 55	16 12	diffuse	

Table 2 (continued)

(1)	(2)	(3)	(4)	(5)	(6)	(7)	(8)	
Z 51		87		$1^h30^m46^s.5$	30°10'37"	7 7	starlike	
Z 52				1 30 51.5	30 05 47	14 7		
Z 52A				1 30 52.7	30 05 40	16 12	core+extension	
Z 53				1 30 57.5	30 17 23	8 12		
Z 54				1 29 41.5	30 17 13	16 16	diffuse	
Z 55				1 29 49.5	30 25 48	18 7		R
Z 56				1 29 51.7	30 25 32	8 16	diffuse	
Z 57				1 29 50.1	30 25 13	8 8		
Z 58				1 29 57.3	30 29 18	8 7		
Z 59				1 29 53.0	30 24 56	7 20	core+extension	
Z 60				1 29 57.3	30 25 27	5 4	diffuse	
Z 61				1 29 53.7	30 20 23	6 8		
Z 62				1 29 55.2	30 20 42	8 11		
Z 63				1 29 57.6	30 18 47	14 12		
Z 64	275			1 30 03.9	30 22 50	14 14	bubble	
Z 64A				1 29 54.6	30 23 28	4 3	starlike	
Z 65				1 30 07.8	30 24 53	6 6	diffuse	
Z 65A				1 31 01.5	30 28 35	16 14		
Z 66				1 30 10.1	30 26 07	8 14	diffuse	
Z 67				1 30 10.2	30 25 50	16 10	diffuse	
Z 68				1 30 16.3	30 25 42	8 8	diffuse	
Z 69	276			1 30 04.8	30 22 30	22 18		
Z 69A				1 30 03.9	30 21 20	32 32	bubble	
Z 70				1 30 07.9	30 24 05	8 4		*
Z 71				1 30 08.0	30 23 45	10 16	diffuse	
Z 72				1 30 03.0	30 17 44	5 5		
Z 73				1 30 04.2	30 15 17	24 20	diffuse	
Z 73A				1 30 03.1	30 14 15	60 60	diffuse bubble	
Z 74				1 30 07.1	30 15 30	9 24		
Z 75				1 30 12.0	30 19 52	16 24		
Z 75A				1 30 11.5	30 19 30	18 20		
Z 76				1 30 07.6	30 16 55	4 10		
Z 77				1 30 11.8	30 18 24	12 24		R
Z 78				1 31 13.3	30 22 34	20 14	diffuse	R
Z 78A				1 30 11.7	30 18 38	8 10		
Z 79				1 30 17.6	30 23 00	8 112		R
Z 80				1 30 46.5	30 25 34	6 12		
Z 81				1 30 52.1	30 23 04	24 32		R
Z 82				1 30 20.8	30 24 05	20 28		
Z 83				1 30 22.0	30 23 50	5 28	core+extension	
Z 84		48		1 30 24.2	30 24 05	4 4		
Z 85				1 30 23.3	30 23 52	16 6		
Z 85A				1 30 37.8	30 23 18	10 8		
Z 86				1 30 23.0	30 23 15	20 12		
Z 86A				1 30 38.5	30 23 53	28 48	diffuse	
Z 87				1 31 07.2	30 26 37	18 20		R
Z 88				1 30 15.3	30 15 37	6 6	starlike	R
Z 89				1 29 47.8	30 35 55	4 4	diffuse	
Z 90				1 30 00.7	30 30 27	4 4	starlike	
Z 91		26		1 30 03.3	30 34 55	4 4	starlike	
Z 92				1 30 06.8	30 28 30	6 6		
Z 93				1 30 17.1	30 30 36	11 16		
Z 94				1 30 19.3	30 41 17	4 4		
Z 95				1 30 20.1	30 34 33	28 28	diffuse bubble	R
Z 96	605			1 30 20.8	30 33 55	36 11	diffuse arc	
Z 97	605			1 30 21.2	30 33 02	7 7	diffuse	R
Z 98				1 31 25.2	30 22 20	20 12		
Z 99				1 30 24.2	30 40 53	60 24		
Z 100	290			1 30 23.5	30 30 11	36 36	bubble	R
Z 101	605			1 30 22.5	30 33 32	56 56	bubble	
Z 102	605	47		1 30 23.8	30 33 53	12 12		
Z 103				1 30 26.1	30 35 35	5 5		
Z 104				1 30 24.5	30 38 19	20 19	diffuse	
Z 104A				1 30 28.0	30 38 25	24 10		
Z 105				1 30 28.3	30 39 05	14 15	diffuse	
Z 106				1 30 29.5	30 39 48	16 16	diffuse	
Z 107				1 30 29.7	30 42 50	6 6		
Z 108				1 30 34.0	30 32 12	12 12		
Z 109				1 30 40.1	30 34 50	6 4		
Z 110		94		1 30 48.4	30 35 54	34 34		
Z 111				1 30 41.0	30 35 09	6 12		
Z 112		86		1 30 46.5	30 35 36	8 8		R
Z 113	228			1 30 17.8	30 19 52	4 4	starlike	
Z 114				1 30 20.0	30 19 27	16 16		
Z 115	228			1 30 22.0	30 19 01	22 28		R
Z 116	228			1 30 23.3	30 18 48	14 15		R
Z 117				1 30 22.8	30 15 22	20 24		
Z 121		50		1 30 28.0	30 15 52	8 8		
Z 122	244			1 30 29.7	30 17 55	8 12		
Z 123	244			1 30 31.3	30 17 28	10 8		
Z 123A				1 30 26.7	30 17 05	14 14	diffuse	
Z 124	244			1 30 33.0	30 17 00	16 12	core+extension	
Z 125				1 30 32.2	30 15 14	16 12	diffuse	
Z 128				1 30 42.5	30 23 19	6 12		
Z 129		65		1 30 34.2	30 16 16	24 14		
Z 129A				1 30 39.0	30 16 12	24 16		
Z 130				1 30 41.7	30 22 07	9 8		
Z 130A				1 30 42.5	30 23 19	6 6		
Z 131				1 30 41.8	30 18 32	12 4	core+extension	
Z 131A				1 30 41.2	30 21 34	7 6	diffuse	
Z 132				1 30 44.7	30 18 00	18 28	diffuse	
Z 132A				1 30 46.2	30 17 33	6 6		
Z 133				1 30 49.9	30 19 04	19 32	double arc	
Z 134				1 30 48.4	30 20 52	10 12	diffuse	
Z 135				1 30 49.5	30 21 12	12 14		
Z 136				1 30.50.5	30 21 29	11 12		
Z 137				1 30 49.3	30 14 55	7 7		
Z 138		95		1 30 48.5	30 24 13	6 6	starlike	
Z 139				1 30 53.3	30 10 31	7 7		
Z 140				1 31 00.5	30 25 35	14 11		

(1)	(2)	(3)	(4)	(5)	(6)	(7)	(8)	
Z 141				$1^h30^m59^s.6$	30°18'37"	9 9		
Z 141A				1 31 04.0	30 18 38	11 7	core+halo	
Z 141B				1 31 05.5	30 18 30	12 15		
Z 143				1 31 00.4	30 20 10	9 20		
Z 143A				1 31 05.2	30 19 24	10 10		
Z 144				1 31 00.5	30 15 26	16 12	diffuse	
Z 145				1 31 01.0	30 14 02	28 28	diffuse bubble	
Z 146				1 31 02.0	30 15 36	16 16	diffuse	
Z 147				1 31 02.0	30 15 18	20 15	diffuse bubble	
Z 148				1 31 03.0	30 13 08	16 16	diffuse	
Z 148A				1 31 05.5	30 12 22	72 68	ring	
Z 149				1 31 05.5	30 17 27	9 5		
Z 150				1 31 02.8	30 20 50	4 4	diffuse	
Z 160				1 31 03.5	30 22 27	20 12		
Z 160A				1 31 03.6	30 21 52	9 16		
Z 171				1 31 10.3	30 25 38	16 8		
Z 171A				1 31 11.6	30 25 17	5 6	starlike	
Z 172				1 31 23.9	30 35 49	16 10		*
Z 173				1 31 19.4	30 35 29	10 12	core+halo	
Z 174	701			1 31 12.0	30 15 03	6 5		
Z 175	701			1 31 20.0	30 15 25	10 10	core+extension	
Z 176	701			1 31 13.0	30 16 02	20 24	core+halo	
Z 180				1 31 13.5	30 21 30	15 9		
Z 181				1 31 11.5	30 16 38	17 16		
Z 182				1 31 18.7	30 17 25	5 5	starlike	
Z 183				1 31 19.3	30 15 35	7 7		
Z 184				1 31 23.5	30 19 53	12 12	core+halo	
Z 184A				1 31 20.2	30 18 57	8 6		
Z 185				1 31 24.6	30 20 03	8 12	diffuse	
Z 187				1 31 26.0	30 15 40	12 16		
Z 188				1 31 29.3	30 15 10	9 20	core+extension	
Z 189				1 31 31.2	30 15 52	6 6		
Z 190				1 31 35.0	30 15 58	24 24	diffuse ring	
Z 192				1 31 30.6	30 18 37	8 5		*
Z 193	290			1 30 25.0	30 29 24	12 12		
Z 194	290			1 30 22.0	30 29 53	20 16	superposed with star	
Z 195	290	52	I 131	1 30 25.8	30 29 55	18 32	bright rim+absorption	
Z 197	290			1 30 28.0	30 29 45	9 20	core+extension	R
Z 198				1 30 27.0	30 29 30	52 52	bubble	
Z 199				1 30 35.0	30 34 46	12 10		
Z 200				1 30 36.5	30 28 07	9 9	diffuse	
Z 201				1 30 38.0	30 30 31	40 36		R
Z 202				1 30 37.8	30 29 42	5 5		
Z 203				1 30 40.3	30 33 52	4 4	diffuse	
Z 204				1 31 19.0	30 23 55	4 36	filament	
Z 205				1 30 38.5	30 26 22	8 12		
Z 206				1 30 39.8	30 25 54	6 6	starlike	
Z 207				1 30 42.2	30 32 06	5 5		
Z 208		171		1 31 21.0	30 23 57	8 8		
Z 209				1 30 44.0	30 27 55	12 8		
Z 210				1 30 44.5	30 29 27	8 6		R
Z 211				1 30 46.3	30 34 04	8 8		
Z 212				1 31 08.5	30 33 43	6 6		
Z 213				1 30 50.3	30 28 50	8 6		
Z 214				1 30 48.8	30 33 40	44 12	diffuse arc	
Z 215				1 30 52.0	30 30 45	5 8		
Z 216				1 30 53.3	30 31 06	16 16		
Z 217				1 30 54.3	30 31 55	28 28		
Z 218				1 30 54.2	30 30 23	6 6		
Z 219				1 30 55.8	30 32 04	12 16		
Z 220				1 30 57.5	30 36 00	10 16		
Z 221				1 30 59.0	30 36 51	8 8		
Z 222				1 31 00.3	30 37 13	8 8		
Z 223				1 31 09.0	30 32 05	8 8		
Z 224				1 31 08.5	30 31 23	3 3	starlike	
Z 224A				1 31 07.8	30 30 45	6 6		
Z 225				1 30 55.0	30 28 22	24 24		
Z 226				1 31 03.5	30 29 48	8 12		
Z 226A				1 30 58.3	30 29 27	10 12		R
Z 227				1 31 15.0	30 30 27	16 12		
Z 228				1 31 03.8	30 31 03	5 8		R
Z 229				1 31 06.7	30 32 30	12 16	diffuse	
Z 230		145		1 31 08.5	30 33 38	8 8		
Z 231				1 31 09.0	30 36 40	12 12	diffuse	
Z 232				1 31 06.2	30 29 42	8 16		
Z 233				1 31 09.0	30 33 12	6 6	starlike	
Z 233A				1 31 09.0	30 33 24	7 7		
Z 234				1 31 10.4	30 34 05	5 5	starlike	
Z 235				1 31 11.5	30 28 24	4 4		
Z 236				1 31 04.0	30 28 05	36 52		R
Z 237				1 31 06.4	30 27 32	3 3	starlike	
Z 238				1 31 09.8	30 27 43	6 12	diffuse	
Z 239				1 31 12.0	30 29 08	8 12	diffuse	
Z 240				1 31 10.8	30 27 00	8 6		*
Z 241				1 31 12.2	30 28 39	5 6	starlike	
Z 242				1 31 13.5	30 28 52	20 24	diffuse	
Z 243				1 31 50.0	30 29 26	10 10	diffuse	
Z 244				1 31 12.8	30 30 43	8 14		
Z 245				1 31 12.0	30 31 16	27 21		
Z 246				1 31 16.0	30 32 39	10 12		
Z 246A				1 31 17.3	30 32 37	8 12		
Z 246B				1 31 19.0	30 32 25	8 10	diffuse	
Z 247		166		1 31 17.0	30 33 38	11 12		
Z 248				1 31 14.5	30 35 28	8 8	diffuse	
Z 249				1 31 17.5	30 34 22	10 10		
Z 250				1 31 21.0	30 33 47	6 5	diffuse	
Z 251				1 31 21.0	30 34 03	8 8		
Z 252				1 31 22.0	30 34 04	8 12	diffuse	
Z 253				1 31 22.3	30 28 00	3 3	starlike	
Z 254				1 31 22.2	30 28 12	5 5		

Table 2 (continued)

(1)	(2)	(3)	(4)	(5)	(6)	(7)	(8)	
Z 255				$1^h31^m21^s.0$	30°26'50"	10 8	diffuse	
Z 256				1 31 25.0	30 29 07	40 32	diffuse ring	
Z 257				1 31 23.3	30 30 47	6 6		
Z 258				1 31 24.3	30 32 05	7 10		
Z 259				1 31 25.0	30 34 25	4 4	diffuse	
Z 260				1 31 25.0	30 34 15	12 8		
Z 261				1 31 30.0	30 33 20	18 12		
Z 262				1 31 35.5	30 33 37	4 24	arc	
Z 263				1 29 55.0	30 09 40	68 76	bubble	
Z 265	205			1 30 46.8	30 15 45	9 9		R
Z 266				1 30 46.3	30 17 00	11 16		
Z 267				1 30 43.5	30 16 20	19 12		
Z 270				1 31 26.8	30 33 13	8 8		
Z 271				1 31 27.5	30 36 18	36 24	diffuse	
Z 272				1 31 25.2	30 23 32	24 28	diffuse	
Z 273				1 31 24.2	30 21 26	7 5		
Z 273A				1 31 26.9	30 21 17	15 15		
Z 274				1 31 28.4	30 26 05	20 12	diffuse	
Z 274A				1 31 32.0	30 25 20	20 19	diffuse	
Z 275				1 31 27.1	30 27 57	12 12	diffuse	
Z 276				1 31 29.7	30 28 48	4 4		
Z 277				1 31 29.5	30 29 45	10 10	diffuse	
Z 279				1 31 32.4	30 31 50	10 10		
Z 280				1 31 31.2	30 30 15	56 48	diffuse bubble	R
Z 281				1 31 42.0	30 32 53	12 12	core+halo	
Z 282				1 31 42.5	30 34 03	16 12	diffuse	
Z 283				1 31 45.5	30 33 05	14 8	diffuse	
Z 284				1 31 47.5	30 31 34	12 12		
Z 284A				1 31 48.4	30 31 07	8 10		
Z 285				1 30 41.8	30 44 17	60 60	diffuse bubble	
Z 286				1 30 48.0	30 44 15	6 6		
Z 286A				1 30 47.0	30 45 08	48 10	bubble	R
Z 287				1 30 48.8	30 47 20	16 16		
Z 288				1 31 03.3	30 41 58	12 14		
Z 289				1 31 07.4	30 45 33	12 10		
Z 290				1 31 13.1	30 48 07	8 8		
Z 291				1 31 14.5	30 46 58	12 12		
Z 292				1 31 46.3	30 30 43	22 20	diffuse	
Z 293				1 31 15.8	30 47 40	12 10		
Z 294				1 31 15.7	30 44 23	4 4		
Z 295				1 31 14.3	30 39 08	10 10		
Z 296				1 31 20.5	30 48 10	8 8	diffuse	
Z 297				1 31 23.3	30 55 10	68 68	diffuse ring	
Z 298				1 31 22.2	30 47 58	24 16	core+halo	
Z 299		178		1 31 24.0	30 48 42	7 7		
Z 300				1 31 23.2	30 46 57	6 6		
Z 301				1 31 29.0	30 49 21	18 20	diffuse	
Z 302				1 31 34.5	30 41 05	20 8	diffuse	
Z 303				1 31 36.3	30 41 10	12 8	diffuse	
Z 304				1 31 51.2	30 28 32	32 20	diffuse	
Z 305				1 31 25.5	30 38 23	10 40	diffuse	R
Z 305A				1 31 24.8	30 38 30	8 18	diffuse	
Z 306				1 31 19.2	30 46 35	20 24		
Z 307				1 30 57.7	30 12 00	12 10		
Z 308	760	139		1 31 06.2	30 04 38	8 6		
Z 309	760	140		1 31 06.7	30 04 24	5 5		
Z 311				1 31 07.7	30 13 26	6 6	starlike	
Z 312	759			1 31 07.5	30 06 57	10 12		
Z 313	759			1 31 07.3	30 07 15	10 12	diffuse	
Z 314				1 31 08.3	30 09 52	12 10	core+halo	
Z 315				1 31 07.5	30 05 06	12 12	diffuse bubble	*
Z 316		148		1 31 10.8	30 07 42	10 24	diffuse	
Z 317				1 31 12.0	30 07 20	8 8	diffuse	
Z 318				1 31 12.2	30 07 39	7 7		
Z 319				1 31 12.3	30 00 45	20 20	diffuse	
Z 320				1 31 16.2	30 08 24	9 8	diffuse	
Z 321				1 31 19.0	30 08 04	4 4		
Z 322				1 31 21.3	30 10 37	6 6		
Z 322A				1 31 25.0	30 10 28	10 10	core+halo	
Z 323				1 31 21.0	30 06 43	60 60	bubble	
Z 324				1 31 22.5	30 11 55	12 8	diffuse	
Z 325				1 31 24.2	30 12 25	28 28	diffuse halo	
Z 326				1 31 25.0	30 07 53	10 10		
Z 327				1 31 26.4	30 12 27	12 6	diffuse	
Z 328				1 31 26.7	30 12 50	8 8	diffuse	
Z 329				1 31 30.3	30 08 16	8 8		
Z 330				1 31 34.0	30 10 07	12 12	diffuse	
Z 331				1 31 39.6	30 09 36	4 4	diffuse	
Z 332				1 31 40.0	30 08 32	6 6		
Z 334		219		1 31 53.1	30 08 43	4 4		
Z 338				1 31 40.0	30 20 02	16 16	diffuse	
Z 339				1 31 40.8	30 20 26	12 14	diffuse	
Z 340				1 31 42.7	30 22 05	24 24	diffuse bubble	
Z 341				1 31 43.0	30 20 12	8 12	diffuse	
Z 343				1 31 35.0	30 23 48	3 3	starlike	
Z 344				1 31 37.8	30 24 22	8 8	diffuse	
Z 345				1 31 43.9	30 24 45	10 40	diffuse arc	
Z 347				1 31 50.2	30 23 48	24 16	diffuse ring	
Z 348	757			1 31 55.0	30 27 23	8 12	diffuse	*
Z 349				1 31 54.8	30 28 00	8 4	diffuse	
Z 350	757			1 31 56.0	30 27 12	8 6		
Z 352				1 31 55.3	30 23 27	4 4	diffuse	
Z 353				1 31 48.8	30 17 12	6 6		
Z 354				1 31 51.0	30 18 37	8 8	diffuse	
Z 356				1 31 52.9	30 17 15	6 6		
Z 357				1 31 51.3	30 15 41	8 8		
Z 358				1 31 54.1	30 16 43	8 8		
Z 358A		221		1 31 56.1	30 17.17	2 2	starlike faint	
Z 359				1 32 01.5	30 20 48	32 30	bubble	
Z 360				1 31 53.4	30 22 25	68 48	diffuse	R
Z 361				$1^h32^m03^s.2$	30°20'05"	12 12	core+halo	
Z 362				1 32 11.8	30 23 01	36 34	bubble	
Z 363				1 32 11.0	30 22 03	4 8	core+halo	
Z 364				1 32 14.0	30 21 50	30 31	bubble	
Z 365				1 32 09.0	30 15 57	6 6		
Z 366	755			1 32 16.0	30 25 05	20 16		
Z 366A	755			1 32 16.5	30 25 45	12 16		R
Z 367				1 32 21.5	30 26 35	24 24	core+halo	
Z 368				1 31 25.5	30 39 18	10 8	diffuse	
Z 370				1 31 35.5	30 37 33	36 36	diffuse bubble	
Z 371				1 32 11.0	30 26 34	5 5	starlike	
Z 372				1 31 35.2	30 39 40	16 17		
Z 373				1 31 35.5	30 39 25	13 13	diffuse	
Z 374				1 31 38.5	30 39 10	12 20		
Z 375				1 31 39.3	30 44 15	14 10	diffuse	
Z 376				1 31 39.7	30 44 02	4 4	core+halo	
Z 377		205		1 31 41.8	30 42 07	10 10	starlike bright	
Z 378		207		1 31 42.3	30 42 18	12 10	starlike bright	
Z 379				1 31 45.5	30 41 27	7 7	diffuse	
Z 380				1 31 45.5	30 41 48	3 3	diffuse	
Z 381				1 31 45.5	30 35 44	4 4	starlike	
Z 382				1 31 49.3	30 44 55	6 7		
Z 383				1 31 50.0	30 41 55	60 8	diffuse extension	R
Z 384				1 31 50.5	30 36 15	48 48	diffuse halo	
Z 385				1 31 53.5	30 34 03	20 18	bubble	
Z 386				1 32 01.1	30 40 08	32 36	diffuse halo	
Z 387	558			1 32 01.4	30 39 00	7 6		
Z 388	558			1 32 02.3	30 39 05	8 11		
Z 389		223		1 32 02.8	30 38 41	5 5	starlike	
Z 390				1 32 03.0	30 39 35	7 12	core+halo	
Z 391				1 32 11.0	30 35 07	7 7	diffuse	
Z 392				1 32 12.7	30 45 20	6 5		
Z 393		2		1 29 38.0	30 10 08	4 4	starlike	
Z 394		5		1 29 44.9	30 12 05	3 3	starlike	
Z 395		9		1 29 50.5	30 07 00	15 15	starlike+diffuse halo	
Z 396		15		1 29 53.0	30 05 45	3 3	starlike	
Z 397		17		1 29 53.6	30 04 01	5 5	starlike	
Z 398		18		1 29 54.5	30 19 54	3 3	starlike	
Z 399		19		1 29 55.3	30 06 33	3 3	starlike	
Z 400		20		1 29 55.5	30 19 54	4 4	starlike	
Z 401		23		1 29 57.0	30 26 16	6 6	starlike	
Z 402		25		1 29 59.8	30 10 30	3 3	starlike	
Z 403		37		1 30 18.4	30 15 37	6 6	starlike	
Z 405		159		1 31 13.0	30 42 44	6 6	starlike	
Z 406		164		1 31 16.3	30 07 22	2 2	starlike	
Z 407		172		1 31 21.7	30 27 02	6 5	starlike	*
Z 409		16		1 29 53.2	30 06 58	6 6	starlike	
Z 410				1 29 50.0	30 10 00	8 8	diffuse	

Notes to Table 2

15 Filament parallel to the spiral arm between 15 and 19
16 Filament between 16 and 27
19 See 15
20 Filament W
27 Filament to 14, 16, 25
36 Absorbing cloud NE of 36
38 Absorbing cloud between 38 and Z 81
41 Absorbing cloud S
42 Absorbing cloud between 42 and 1008; possible TT structure
45 Filament between 45 and 1007
47 Absorbing cloud between 47 and 51
48 Filament between 48 and Z 138
49 Rich filamentary extensions
51 Filament between 51 and 44, absorbing cloud between 51 and 47
63 Filament between 63 and Z 236
83 Filament between 83 and Z 98
88 Filament and possible TT structure
90 Filament EW
91 Filament between 91 and 97; filament parallel to the spiral arm to halfway between 751 and 100
202 Embedded in a complex filamentary area of about 1.5 in diameter centerd $1^h30^m49^s + 30°16'03''$
203 Idem
204 Idem
216 Filament and absorbing cloud
218 Bright rim; absorbing cloud N and TT structure S

Notes to Table 2

231 Complex filamentary structure between 231, 233, and 237
233 See 231
237 See 231
239 Complex filamentary structure between 239 and 237
247 Dark cloud W
249 Possible shock wave
256 Two filaments E
261 Possible shock wave
264 Concentric filament SW
269 Filamentary loop between 269, 270, and Z 10
270 See 269
274 Absorbing cloud in the NE and 2 TT structures
281 Dark cloud N
301 Very long filaments between 301 and Z 228 and between 301 and Z 226A
632 TT structure
641 Absorbing cloud S + loop
643 Bubble + bright rims
650 Absorbing cloud N
660 Extension to 651, patchy
663 Filamentary area
664 See 663
666 Filamentary area
667 See 666 and 691
680 Filaments between 680 and 748
683 Filament E
684 Filament
687 Filament midway 687 and 682
688 Filament on E and W sides
691 Absorbing cloud between 667 and 691
710 Filamentary structures around
711 Idem
712 Idem
714 Absorbing cloud, bright rim
734 TT structure
740 Absorbing cloud SE
749 Limited by absorbing clouds
758 Filaments NE and between 758, 148, and 148A
1007 Filaments between 45 and 1007
Z 1A Includes regions 6, 7A, and 7B of Boulesteix et al. 1974)
Z 14 Filaments between Z 14 and 27
Z 19 Filaments between Z 19 and 15
Z 23A TT structure
Z 25 Complex filamentary and patchy structure between Z 25 and Z 133
Z 30A Filaments between Z 30A and 256
Z 34 Filaments and complex filamentary structure between Z 34 and 227–217 group
Z 55 Absorbing cloud S
Z 77 Absorbing cloud S
Z 78 Partly filamentary
Z 79 Large loop centered on Z 86
Z 81 Absorbing cloud Z 81 and 38
Z 87 Filament
Z 88 In a large area of patchy structure
Z 95 Filament S
Z 97 Filament W
Z 100 Filament between Z 100 and 91; absorbing cloud S possible shock wave
Z 112 TT structure
Z 115 TT structure or bright rim
Z 116 See Z 115
Z 197 Possible TT structure
Z 201 Filament
Z 210 Filament w
Z 226A See 301
Z 228 See 301
Z 236 2 filaments S, one between Z 236 and 63
Z 265 See 202
Z 280 Filaments and patchy structure up to 680
Z 286A Double bubble with 640
Z 305 In filamentary area
Z 360 Includes regions 727 and 728 of Boulesteix et al. (1974)
Z 366A Filaments to Z 371 and 754
Z 383 Extended filament N

Identification of point-like nebulae was conducted with the help of comparison plates obtained in the continuum adjacent to Hα at the focus of the 1.2-m telescope of the Observatoire de Haute-Provence. This has permited to avoid mis-identifications with stars in the case of starlike objects. In particular 3 previously identified regions (BCLMP) have been eliminated for this reason. Some ambiguous cases could be resolved owing to the GRISM observations of Lequeux et al. (1986).

A total of 410 new H II regions have been identified. They are listed in Table 2, together with the nebulae identified by BCLMP. Note that one of those regions (region 273) is not visible in the 6-m survey because it is located in the missing area discussed above. It is not drawn in the identification chart but is included in the listing of Table 2.

The information contained in Table 2 is as follows:

– Column 1 lists the reference numbers given to individual H II regions as shown in the charts.

The regions revealed by the present survey are identified by a number preceded by the letter Z. To the others, we have assigned the same number as in the BCLMP catalogue.

– Column 2 gives for the new regions, identification with the reference number of the previous survey. This occurs mainly when several Z-regions are identified in place of a single one in BCLMP, or, in very few cases, when we assign a single Z-number to a complex where BCLMP identified several distinct nebulae.

– Column 3 gives identification with the reference numbers of Lequeux et al. (1986).

– Column 4 gives identification with the NGC and IC numbers.

– Columns 5 and 6 give the position of the center of the areas covered by individual H II regions in 1950.0 equatorial coordinates. These positions have been obtained by reference to a very accurate grid of coordinates constructed by Dubout (1984) using the positions of three reference stars and those of star clusters as given by Karimova and Sharov (1981). We estimate that the positions are accurate to ±1″5 for small regions (<5″) and to a few arc sec for larger ones (depending on the regularity of their shape). For the sake of homogeneity, the positions have been redefined for the nebulae identified in the BCLMP survey. For the region missed by the present survey, the coordinates listed in columns 5 and 6 are those given in the catalogue of BCLMP.

– Column 7 gives the approximate dimensions of the H II regions, in arc sec, as measured by visual inspection of the films. The first number gives roughly the E-W extent of the nebulae and the second number gives the N-S extent. These are only indicative dimensions. Isophotal diameters would have been more accurate, especially in the case of starlike regions whose dimensions are unavoidably very sensitive to the well-known dependence of the observed diameter upon the Hα brightness. Here also, we have redetermined the dimensions of the nebulae identified in the BCLMP survey, except for that the present survey missed. In this case, column 7 lists the diameter previously measured by BCLMP.

– Column 8 gives some remarks. In some cases (noted by "R") more detailed comments are given in the Notes to Table 2. "TT structure" means that the region resembles the "champagne model" of Tenorio-Tagle (1979) and "shock wave" is used for regions having the same kind of morphology as the structures observed in the Orion Nebula by Gull (1974). Symbol * means that the region is mixed with supernovae remnants (Berkhuijsen, 1983; d'Odorico et al., 1982; Viallefond et al., 1986).

3.2. *Ring-like* H II *regions*

A substantial fraction of the H II regions catalogued by BCLMP were found to have a typical ring-like structure. As expected, these regions take the best advantage of the improved spatial resolution of the 6-m observations and are seen in much more detail. Also, for a number of regions detected previously, a ring-like structure, that was missed because of a lack of resolution, is revealed by the 6-m survey. For the same reason, among the newly discovered nebulae, there are a number of faint, ring nebulae that the previous, lower-resolution observations failed to detect.

Some of the ring-like H II regions appear to be single, well-defined rings; others, however, exhibit less idealized and more complex structures. In the latter case, one or several of the following morphological characteristics may occur simultaneously for the same nebula:

– the ring is incomplete and/or more or less disrupted,

– several interlaced rings are present,

– bright knots are visible along the ring as well as "bright rims"

– diffuse emission occurs within the ring,

– diffuse, outlying extensions are detected outside the circular boundary.

The ring diameters are ranging from about 40 pc to 280 pc, assuming a distance of 720 kpc to M 33. Similar large ring-like H II regions are known to occur in the Milky Way (Gum and de Vaucouleurs, 1953; Sivan, 1974) and in most of the nearby galaxies, especially in irregulars and spirals (e.g. Davies et al., 1976; Pellet et al., 1978; de Vaucouleurs, 1978; Lawrie and Kwitter, 1982). As pointed out by Kennicutt (1984), their detection seems to be limited by spatial resolution, and the rings are often seen to resolve into narrow, bright filaments when high-spatial-resolution images are obtained. This resolution effect is well illustrated by comparing the 6-m images of the Hα rings of M 33 with the 1.93-m ones (BCLMP). In the 6-m photographs, the Hα rings appear to be strikingly similar to the rings observed in the Magellanic Clouds (Davies et al., 1976) and the Milky Way. For example, regions 647, Z 263 and Z 362 have the same morphological appearance and roughly the same intrinsic size as respectively the Barnard Loop, the Gum Nebula (Chanot and Sivan, 1983) and Henize N 70.

From galactic and extragalactic studies, it has become clear that the ring-like H II regions are expanding spherical bubbles or shells, whose origin can be generally accounted for by supernovae blasts and/or supersonic stellar winds. Most of them are found to be photoionized by the ultraviolet flux from hot stars. Most of the M 33 bubbles are coinciding with blue associations of Humphreys and Sandage (1980) and, thus, are probably photoionized by the ultraviolet flux from the association stars. Balloon 2000 Å UV images of M 33 are showing UV bright patches at the same position than the large external bubbles (Milliard, 1984). Also, these stars might have been formed in the compressed medium of the expanding shells, in the way described by Sancisi (1974) for the galactic associations Per OB 2 and Sco OB 2 [which also coincide with Hα shells (Sivan, 1974)].

The relationship found by BCLMP between ring diameter and galactocentric radius is confirmed: the diameter of the ring decreases with decreasing galactocentric distance. This trend is accompanied by a deterioration in the quality of the ring: the more perfect rings occur in the outer regions of the galactic disk and the morphology is degraded as one goes inwards. Although more detailed investigations are needed, we suggest that this radial effect results from both the evolution of the bubbles and their interaction with the surrounding medium. It seems that, far from the center, the bubbles may extend up to very large diameters without being disturbed by external influences. On the contrary, in the inner regions, the bubbles are disrupted before they reach large dimensions; this could be accounted for by more or less violent events acting on them such as collisions with denser clouds (e.g. other expanding shells), or the local differential rotation effects of the galaxy.

3.3. *The Hα background*

The present survey reveals a striking new appearance for the so-called, diffuse Hα emission that occurs in the arms and between the arms, outside of the bright, condensed H II regions. This is not a uniform emission: the bright H II regions are embedded in a network of long, complex filaments and loops superposed over large, diffuse areas. A very chaotic medium is revealed, strikingly similar to that observed in the Milky Way (Sivan, 1974) and, in some respects, in the Large Magellanic Cloud (Davies et al., 1976). The observed filaments are typically 1″–4″ thick and up to 3′ long. They are either outlying extensions of bright, condensed H II regions, sometimes connecting two or several regions together, or more isolated features forming more or less well defined enhancements of the general background.

Good examples are given by the area of patchy emission between $\alpha = 1^h29^m55^s$ to $1^h30^m20^s$ and $\delta = 30°15'$ to $30°25'$, and by the two main arms of the galaxy. Similar patchy structure was found in M 31 (see p. 217 in Courtès, 1977).

It should be noted that with the narrow bandpass used in our observations, we can assume that most of the diffuse emission seen in the photographs is nebular and that contribution of unresolved starlight is extremely low. This is supported by the results of previous higher spectral resolution observations made with a Fabry-Perot etalon at the 1.93-m telescope of Observatoire de Haute-Provence (Carranza et al., 1968) and further confirmed at the Palomar 5-m telescope by Courtès, Georgelin and Monnet (see Monnet, 1971).

Figures 11 and 12 are amplified Hα images of large portions of the northern and southern arms respectively, obtained by superpositioning respectively, frames 2 and 11 and frames 3 and 11 (Table 1). In these figures, all the structures of faint surface brightness appear with an enhanced contrast. A number of thin, elongated filaments are seen parallel to the spiral pattern (and thus

possibly aligned along the magnetic field lines), while others are distributed at random between the bright, "classical" H II regions.

In the northern arm, one notes the large dispersion of the H II regions in respect to an idealistic spiral structure. The filaments are roughly parallel oriented each other on considerable length of about 400 pc at the assumed distance of 720 kpc. The rest of the interarm and diffuse ionized gas appears everywhere as patchy structures above the background.

In the southern arm the spiral structure is a continuous evidence, the interarm emission brightness is stronger than the one of the northern arm, with large, relatively uniform areas. The filaments are more linked to the bright H II complexes.

One knows the different nature of the exciting stars populations of the North and South arms, the S arm corresponding to a more recent star formation fitting better with the spiral pattern (Courtès, 1977). The S arm is, owing to its regular morphology, one of the best places to study the density wave velocity and its action on the stellar and gas material (Courtès and Dubout-Crillon, 1971).

The three-dimensional geometry of these filament systems is a priori unknown: they could be actual filaments or sheets of gas or portions of shells. ... However, it is tempting to link them to the ring-like regions discussed in the previous section in an evolutionary sequence, and to imagine that they are portions of disrupted bubbles in a late stage of their evolution. This interpretation would agree with the conclusions of Sivan et al. (1986) for the Galaxy: they found from spectrophotometric observation of the filamentary and diffuse background of a large portion of the Milky Way, that shocks might contribute to the excitation of the galactic interstellar medium, in agreement with the chaotic appearance of this medium.

Whatever the origin of the filaments observed in the Hα background of M33, it should be noted that there exists a remarkable morphological continuity between the different H II region types, in agreement with the general rule pointed out by Kennicutt (1984). No discontinuity is observed over a continuous sequence starting with the bright, circular, "classical" H II regions, running through the more or less well defined bubble regions and ending with the complex filamentary structures.

4. Conclusion

For the first time, thanks to the use of the largest telescope in the world, the various and complex appearance of the ionized gas in an external galaxy (if we except the Magellanic Clouds) was revealed by the photographic Hα survey of M33 presented in this paper.

This survey is a dramatic illustration of the violent energetic events that occur in the interstellar medium. Further quantitative analysis of the photographs shown in this paper and further spectrophotometric and kinematic observations of the filamentary and ring-like structures revealed by the survey might prove to be very useful for a better understanding of the large-scale energetic phenomena involved in the evolution of M33.

Acknowledgements. The observations reported in this paper were carried out at the 6-m telescope owing to an agreement between the USSR Academy of Science and the French Ministère des Relations Extérieures. We would like to express our thanks to both these organisms, as well as to all the colleagues of the Special Astrophysical Observatory, especially to Drs. Kopilov, Afanassiev, Fomenko, Karachentseva, and Karachentsev, whose help and advices contributed to the success of the observations. The technical staff in Zelentchuk is also greatly acknowledged for helping with the instrumentation. Special thanks are due to Dr. Boulesteix whose help was greatly appreciated in many areas. We also wish to thank Dr. Maucherat and F. Bonnarel for helping during an observing run in Zelenchuk and to Drs. Meyssonier, Lequeux and Azzopardi for kindly providing their unpublished data. Finally, the publication of this paper benefits by the help of P. Weber of the Marseille Observatory photographic laboratory who reproduced the identification charts, and by the work of J.-P. Goudal of the photographic laboratory of Laboratoire d'Astronomie Spatiale, who succeeded in the tricky task of reproducing the original films of the survey, with a loss in information as tiny as possible.

References

Berkhuijsen, E.M.: 1983, *Astron. Astrophys.* **127**, 395
Boulesteix, J., Courtès, G., Laval, A., Monnet, G., Petit, H.: 1974, (BCLMP) *Astron. Astrophys.* **37**, 33
Carranza, G., Courtès, G., Georgelin, Y.P., Monnet, G., Pourcelot, A., Astier, N.: 1968, *Ann. Astrophys.*, **31**, 63
Caplan, J., Laval, A.: 1985 (private communication)
Chanot, A., Sivan, J.P.: 1983, *Astron. Astrophys.* **121**, 19
Courtès, G.: 1951a, *Compte-Rend. Acad. Sci. Paris* **232**, 795
Courtès, G.: 1951b, *Compte-Rend. Acad. Sci. Paris* **232**, 1283
Courtès, G.: 1960, *Ann. Astrophys.* **23**, 115
Courtès, G.: 1964, *Astron. J.* **69**, 325
Courtès, G., Dubout-Crillon, R.: 1971, *Astron. Astrophys.* **11**, 468
Courtès, G.: 1972, *Vistas in Astronomy* **14**, 81
Courtès, G.: 1977, Topics in Interstellar Matter, ed. H.Van Woerden, Reidel, Dordrecht, p. 209
Courtès, G., Sivan, J.P., Boulesteix, J., Petit, H.: 1981a, *The Messenger* **23**, 15
Courtès, G., Boulesteix, J., Sivan, J.P.: 1981b, *Compt. Rend. Acad. Sci. Paris* **292**, 1521
Courtès, G., Boulesteix, J., Sivan, J.P., Petit, H., Karachentsev, I.: 1982, Instrumentation for Astronomy with Large Optical Telescopes, ed. C.M. Humphries, Reidel, Dordrecht, p. 67
Cruvellier, P.: 1967, *Ann. Astrophys.* **30**, 1059
Davies, R.D., Elliot, K.H., Meaburn, J.: 1976, *Mem. Roy. Astron. Soc.* **81**, 89
Deharveng, J.M., Pellet, A.: 1970, *Astron. Astrophys.* **9**, 181
de Vaucouleurs, G.: 1978, *Astrophys. J.* **224**, 14
d'Odorico, S., Goss, W.M., Dopita, M.A.: 1982, *Monthly Notices Roy. Astron. Soc.* **198**, 1059
Dubout-Crillon, R.: 1976, *Astron. Astrophys. Suppl. Ser.* **25**, 25
Dubout, R.: 1984 (private communication)
Dubout, R., Laval, A., Maucherat, A., Monnet, G., Petit, M., Simien, F.: 1976, *Astrophys. Letters* **17**, 141
Georgelin, Y.P., Georgelin, Y.M.: 1970, *Astron. Astrophys. Suppl. Ser.* **3**, 1
Gull, T.: 1974, The Amazing Universe, ed. H. Friedman, The Geographical Society Publication
Gum, C.S., de Vaucouleurs, G.: 1953, *Observatory* **73**, 152
Humphreys, R.M., Sandage, A.: 1980, *Astrophys. J. Suppl.* **44**, 319
Karimova, D.K., Sharov, A.S.: 1981, *Soviet Astronomy Letters* **7**, 147
Kennicutt, R.C.: 1979, *Astrophys. J.* **228**, 394
Kennicutt, R.C.: 1984, *Astrophys. J.* **287**, 116
Lawrie, D.G., Kwitter, K.B.: 1982, *Astrophys. J. Letters* **255**, L29

Lequeux, J., Meyssonier, N., Azzopardi, M.: 1986, *Astron. Astrophys. Suppl. Ser.* (in press)
Maucherat, A.J., Dubout-Crillon, R., Monnet, G., Figon, P.: 1984, *Astron. Astrophys.* **133**, 341
Meaburn, J.: 1968, *Astrophys. Space Sci.* **1**, 166
Meaburn, J.: 1970, *Astrophys. Space Sci.* **9**, 206
Milliard, B.: 1984, Thesis, University of Marseille
Monnet, G.: 1971, *Astron. Astrophys.* **12**, 379
Parker, R.A.R., Gull, T.R., Kirschner, R.P.: 1979, An Emission-Line Survey of the Milky Way, NASA, SP 434
Pellet, A., Astier, N., Viale, A., Courtès, G., Maucherat, A., Monnet, G., Simien, F.: 1978, *Astron. Astrophys. Suppl. Ser.* **31**, 439
Reynolds, R.J.: 1980, *Astrophys. J.* **236**, 153
Reynolds, R.J., Roesler, F.L., Scherb, F.: 1974, *Astrophys. J. Letters* **192**, L53
Sabbadin, F., Rafarelli, P., Bianchini, A.: 1980, *Astron. Astrophys. Suppl. Ser.* **39**, 97
Sancisi, R.: 1974, in *Galactic Radio Astronomy*, *IAU Symp.* **60**, eds. F.J. Kerr, S.C. Simonson, Reidel, Dordrecht, p. 65
Sivan, J.P.: 1974, *Astron. Astrophys. Suppl. Ser.* **16**, 163
Sivan, J.P., Stasińska, G., Lequeux, J.: 1986, *Astron. Astrophys.* **158**, 279
Tenorio-Tagle, G.: 1979, *Astron. Astrophys.* **71**, 59
Viallefond, F., Goss, W.M., van der Hulst, J.M., Crane, P.C.: 1986, *Astron. Astrophys. Suppl. Ser.* **64**, 237–246

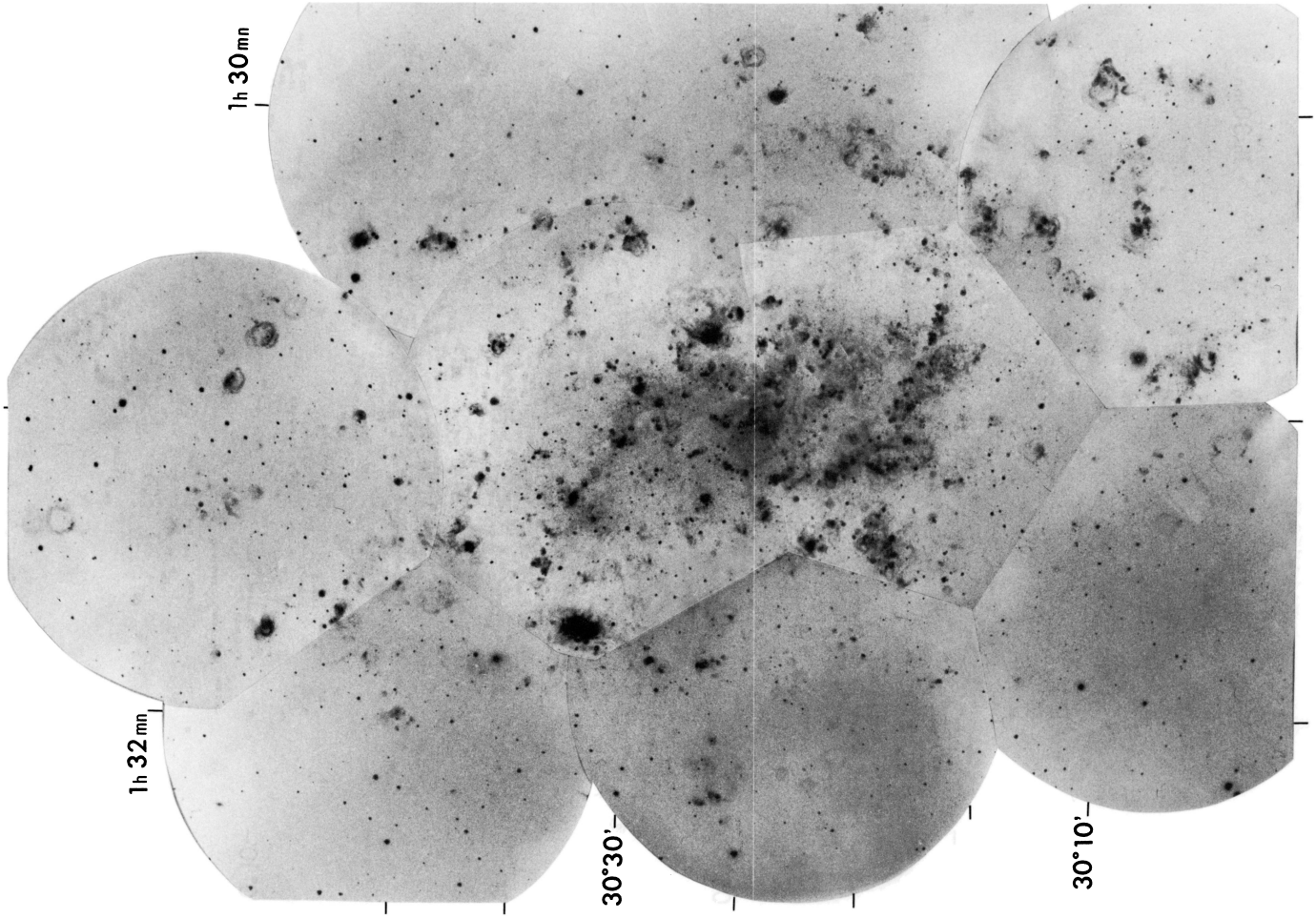

Fig. 1a. Overall view of the Hα photographic survey of M33 conducted at the 6-m telescope. The mosaic is constructed with all the photographs listed in Table 1, except frame n° 11. On the rims of the mosaic are indicated approximate 1950 equatorial coordinates

Astron. Astrophys. 174 (1987)
Springer International

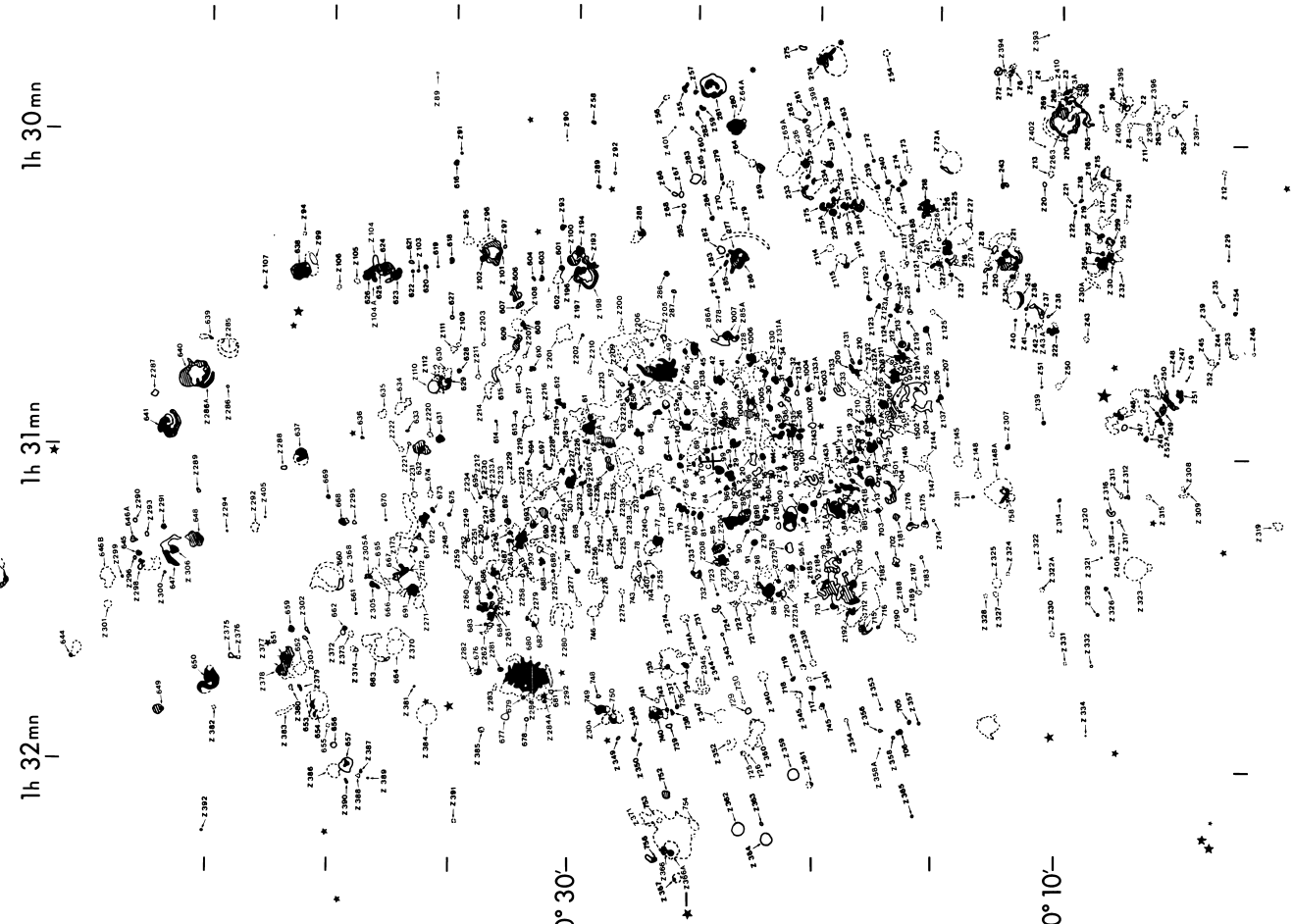

Fig. 1b. Identification chart for the H II regions in Fig. 1a (including all the H II regions listed in Table 2)

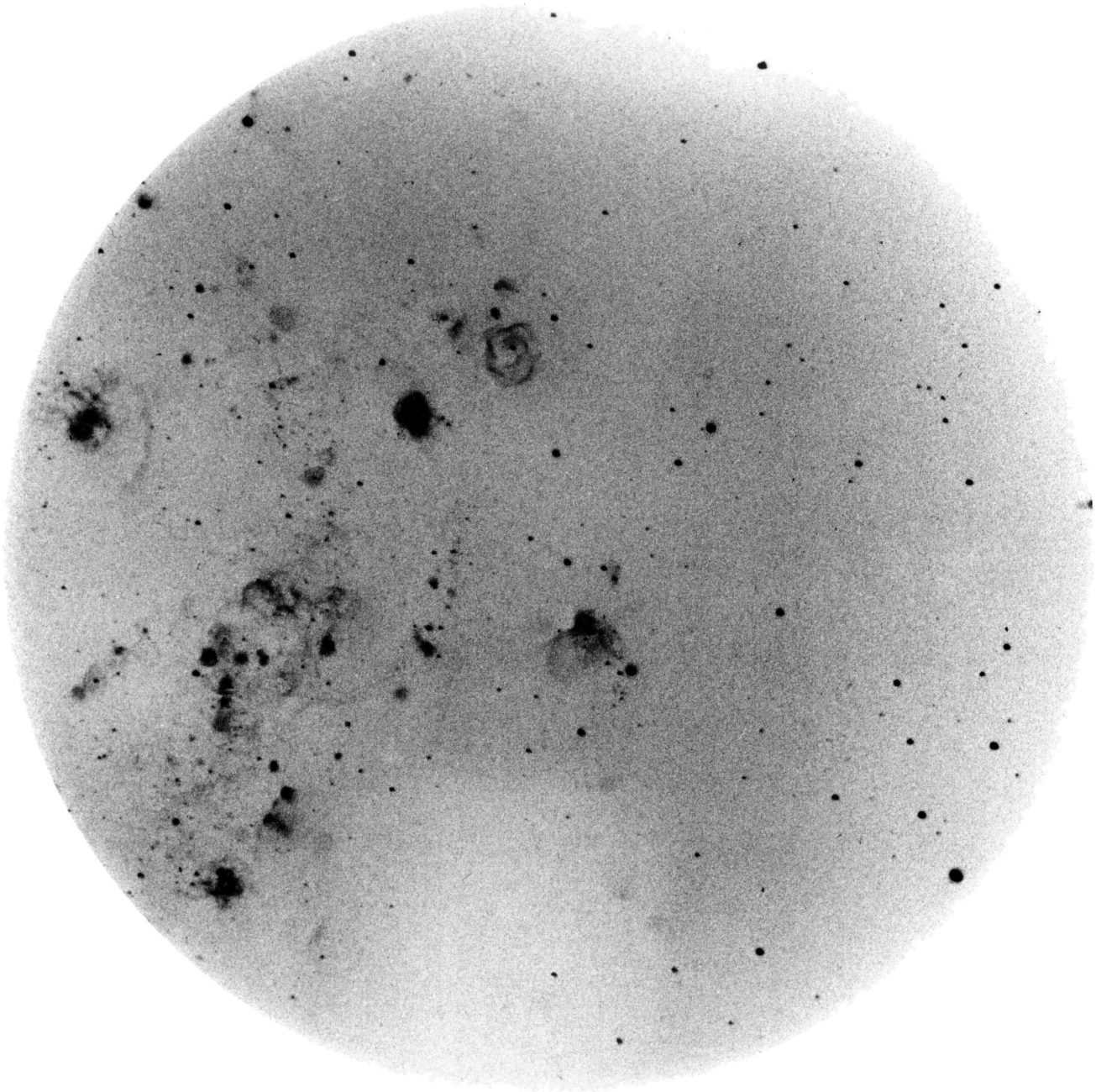

Fig. 2a. Hα photograph of No. 5 (Table 1)

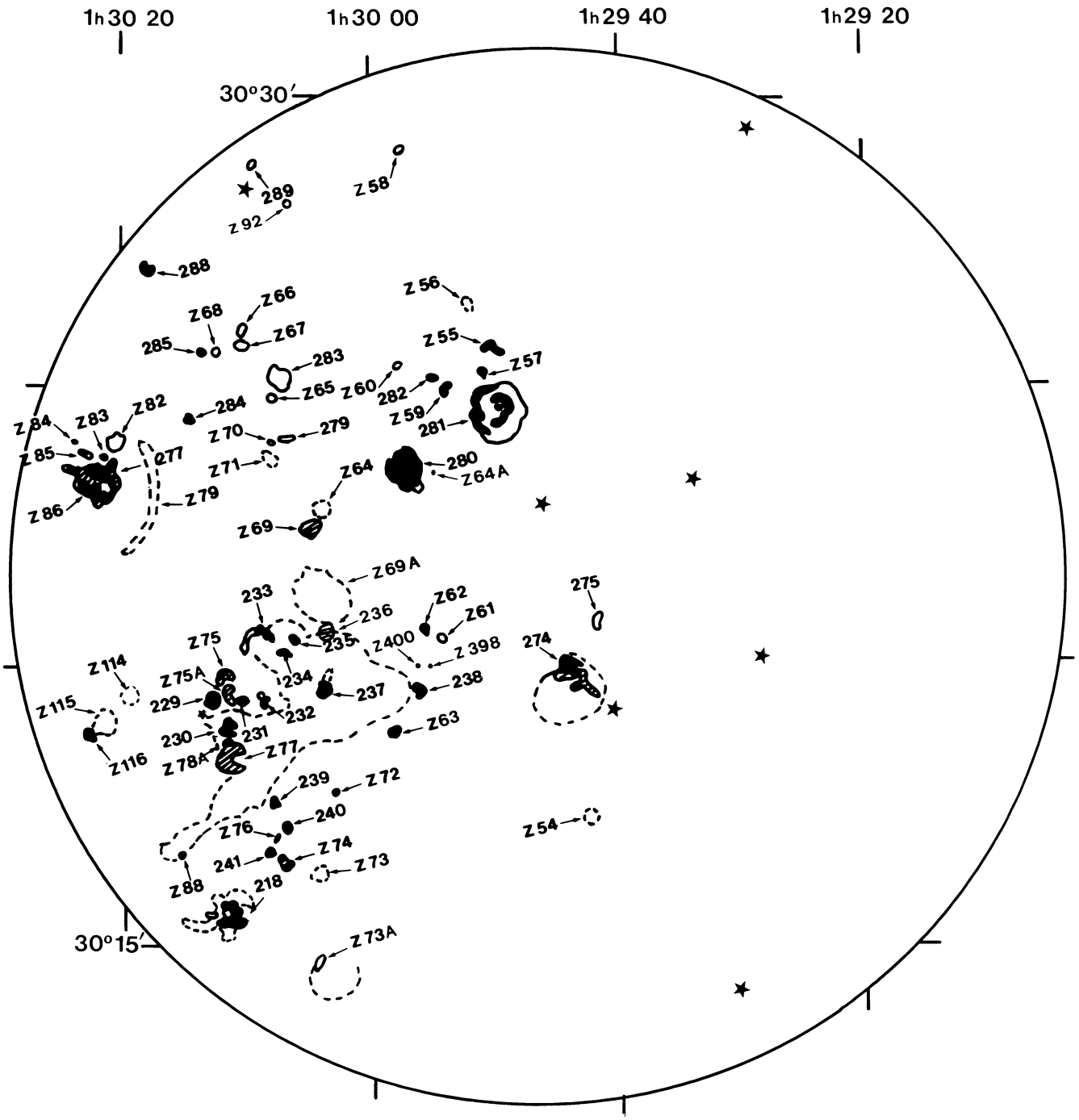

Fig. 2b. Identification chart for the H II regions in Fig. 2a (1950.0 equatorial coordinates)

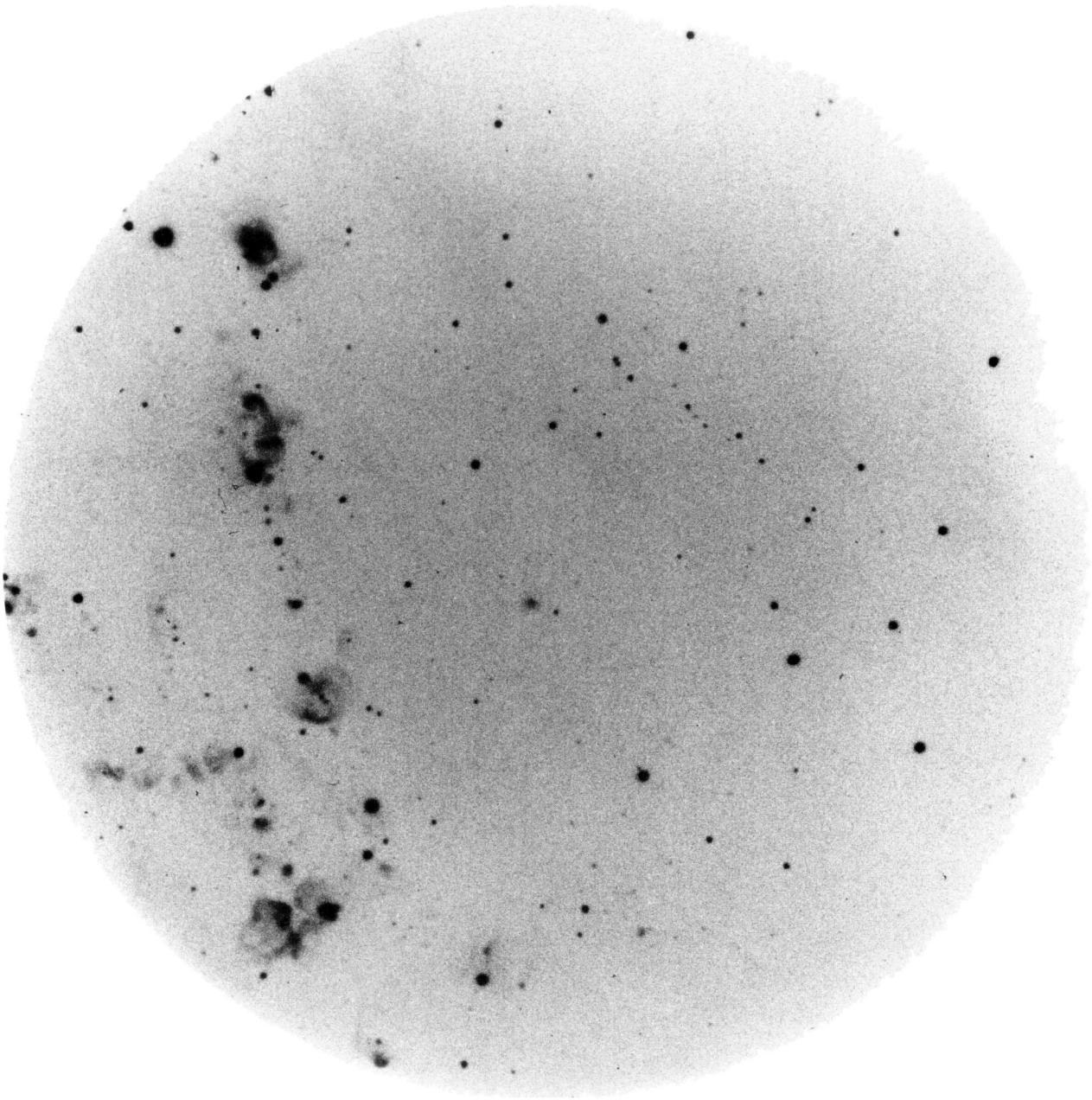

Fig. 3a. Hα photograph of No. 7 (Table 1)

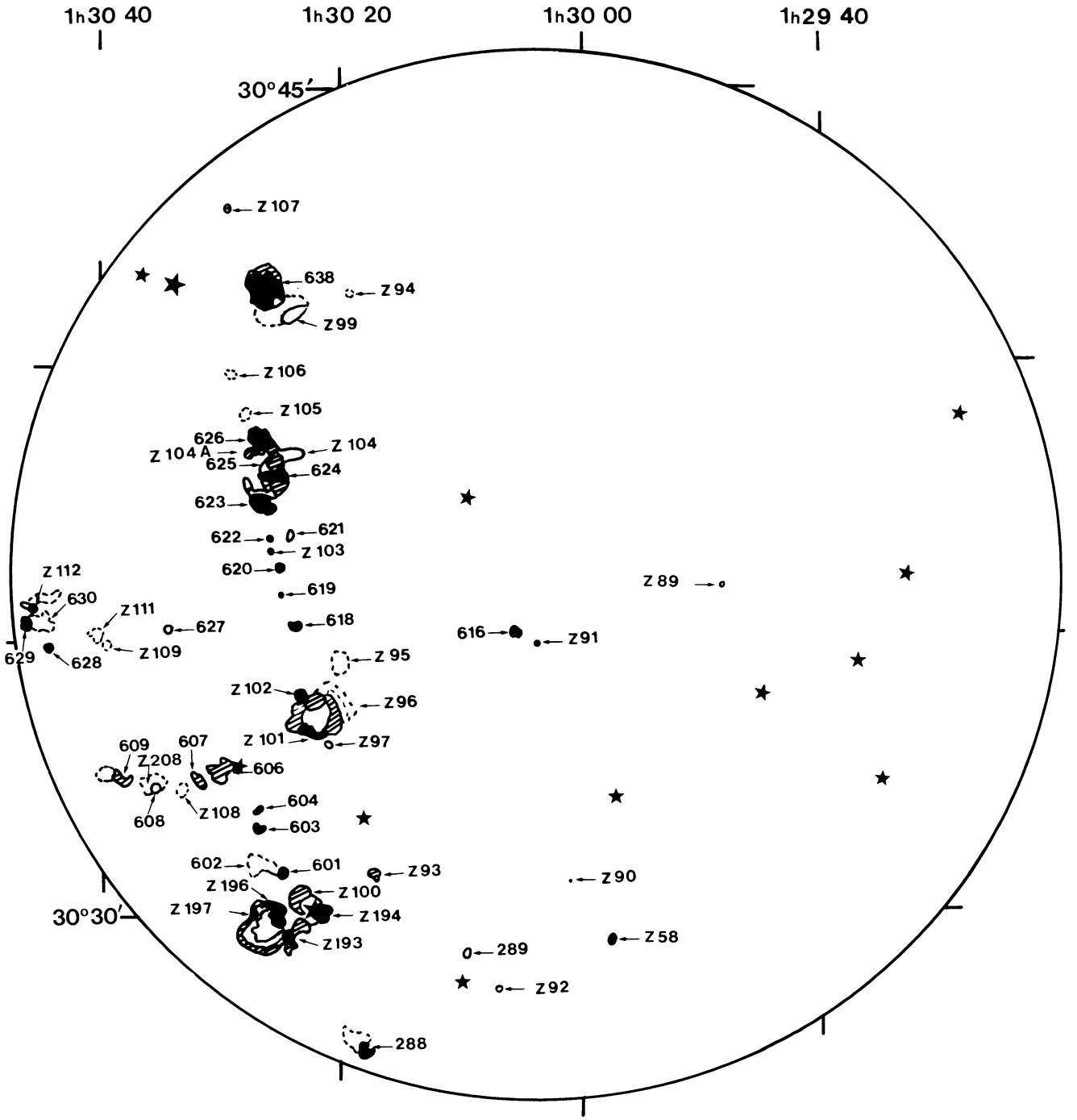

Fig. 3b. Identification chart for the H II regions in Fig. 3a (1950.0 equatorial coordinates)

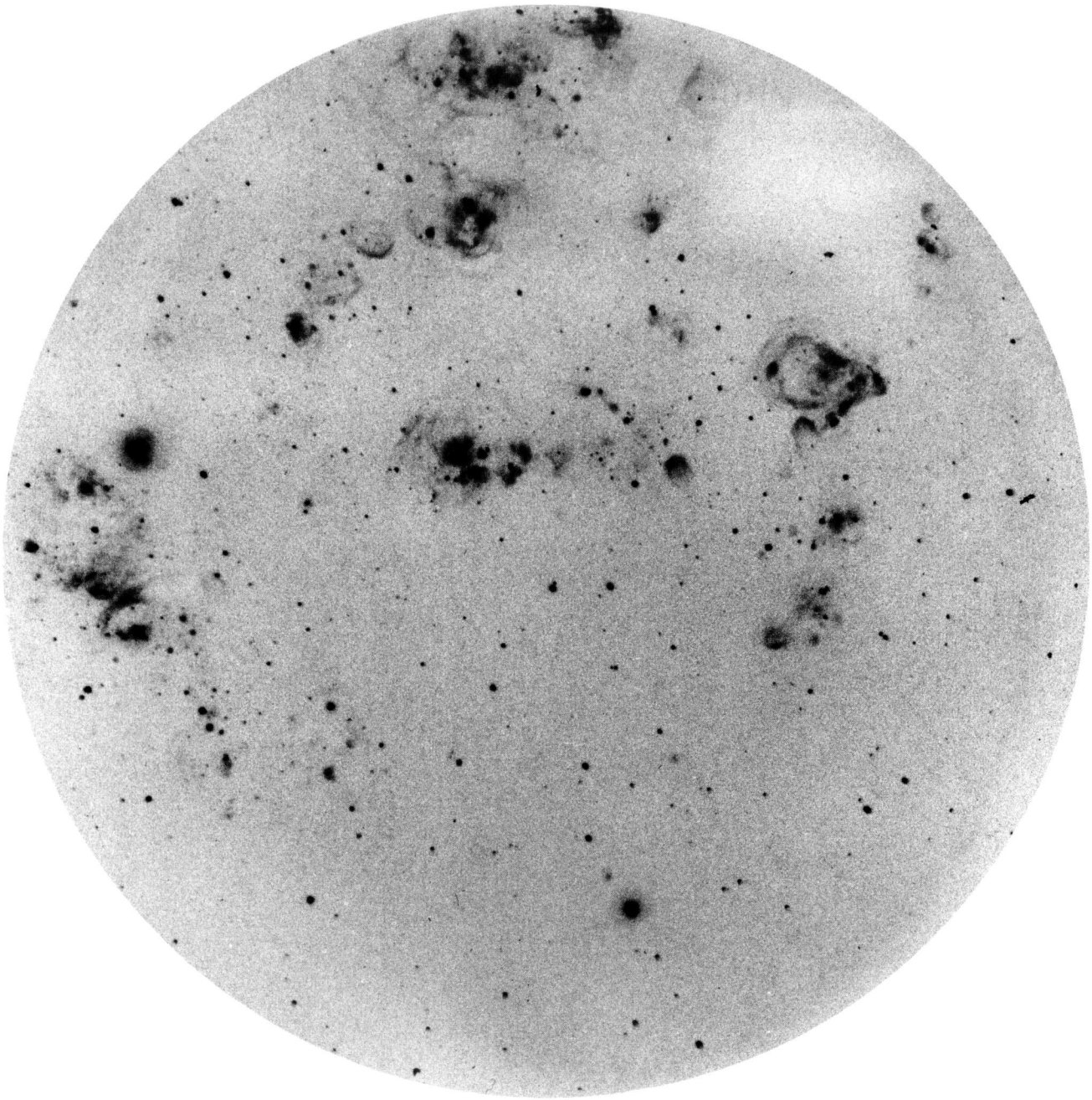

Fig. 4a. Hα photograph of No. 4 (Table 1)

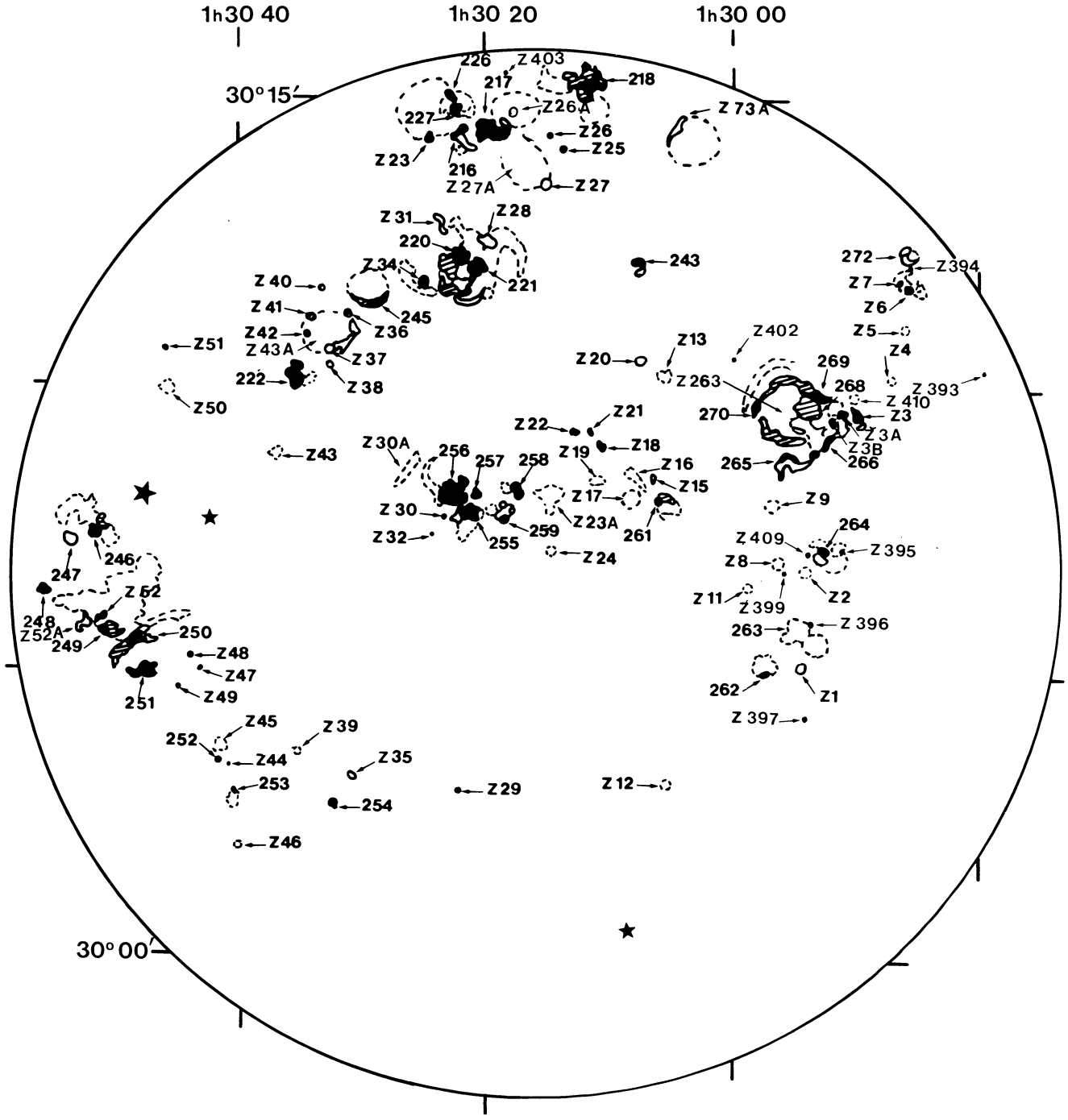

Fig. 4b. Identification chart for the H II regions in Fig. 4a (1950.0 equatorial coordinates)

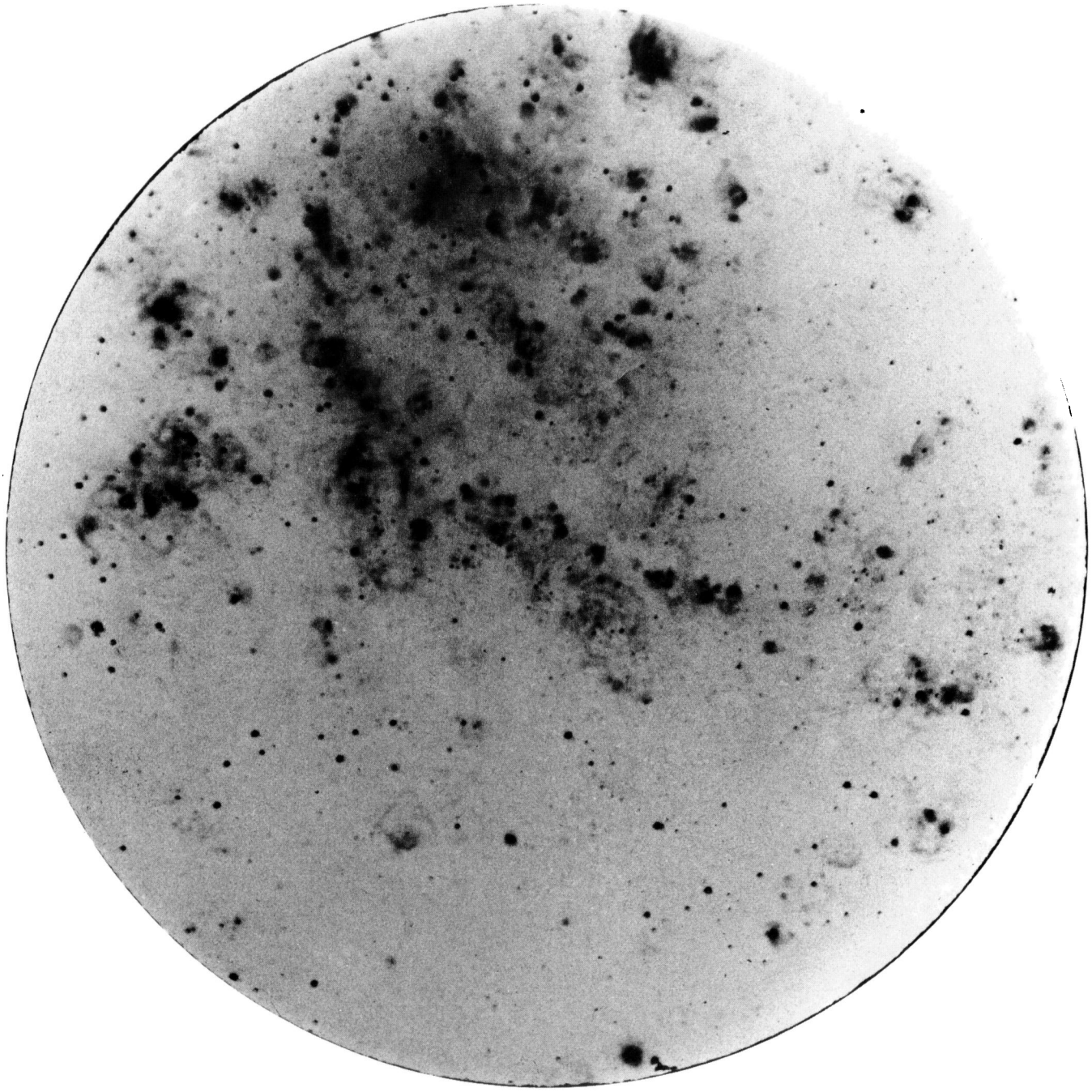

Fig. 5a. Hα photograph of No. 3 (Table 1)

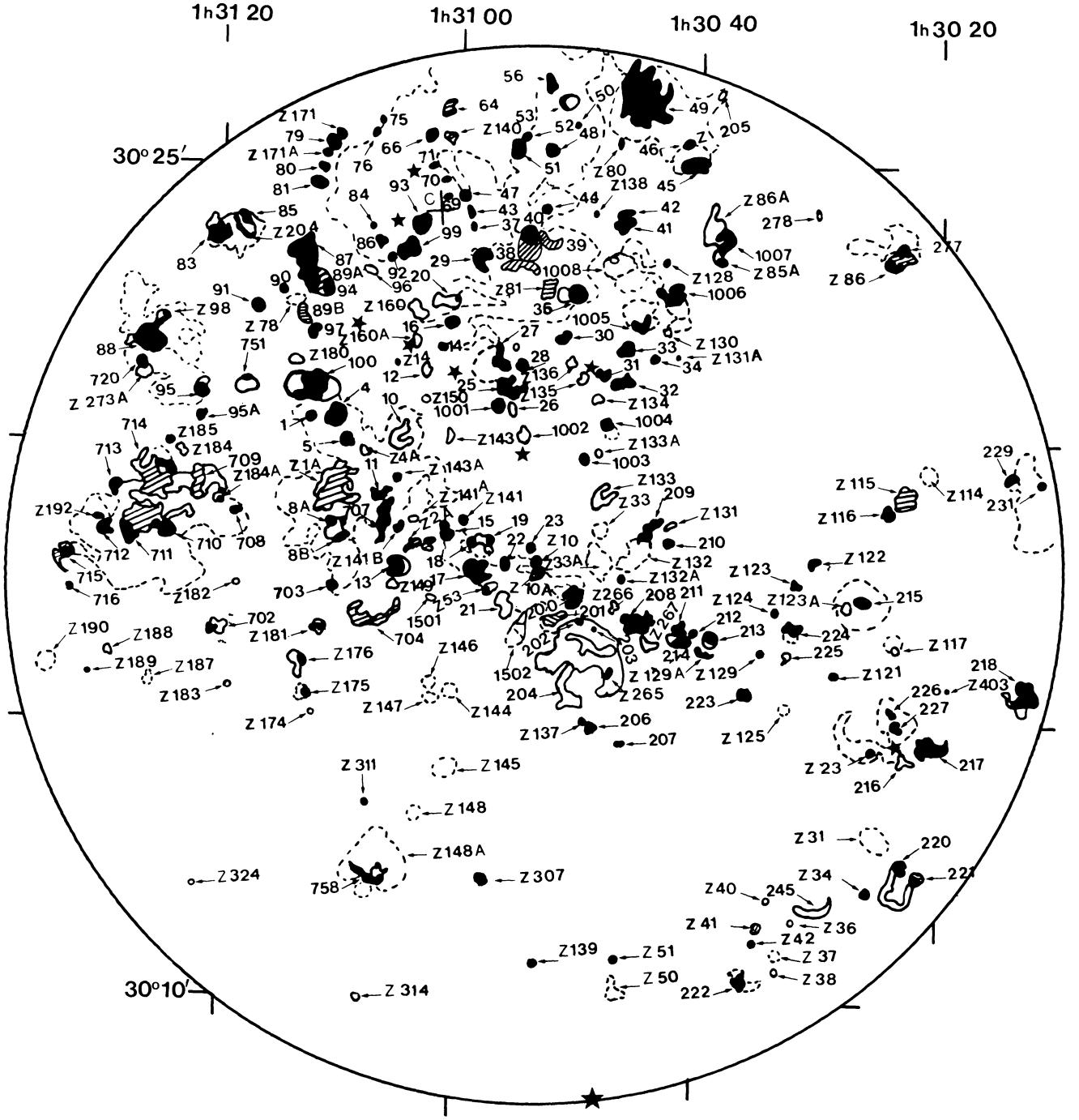

Fig. 5b. Identification chart for the H II regions in Fig. 5a (1950.0 equatorial coordinates)

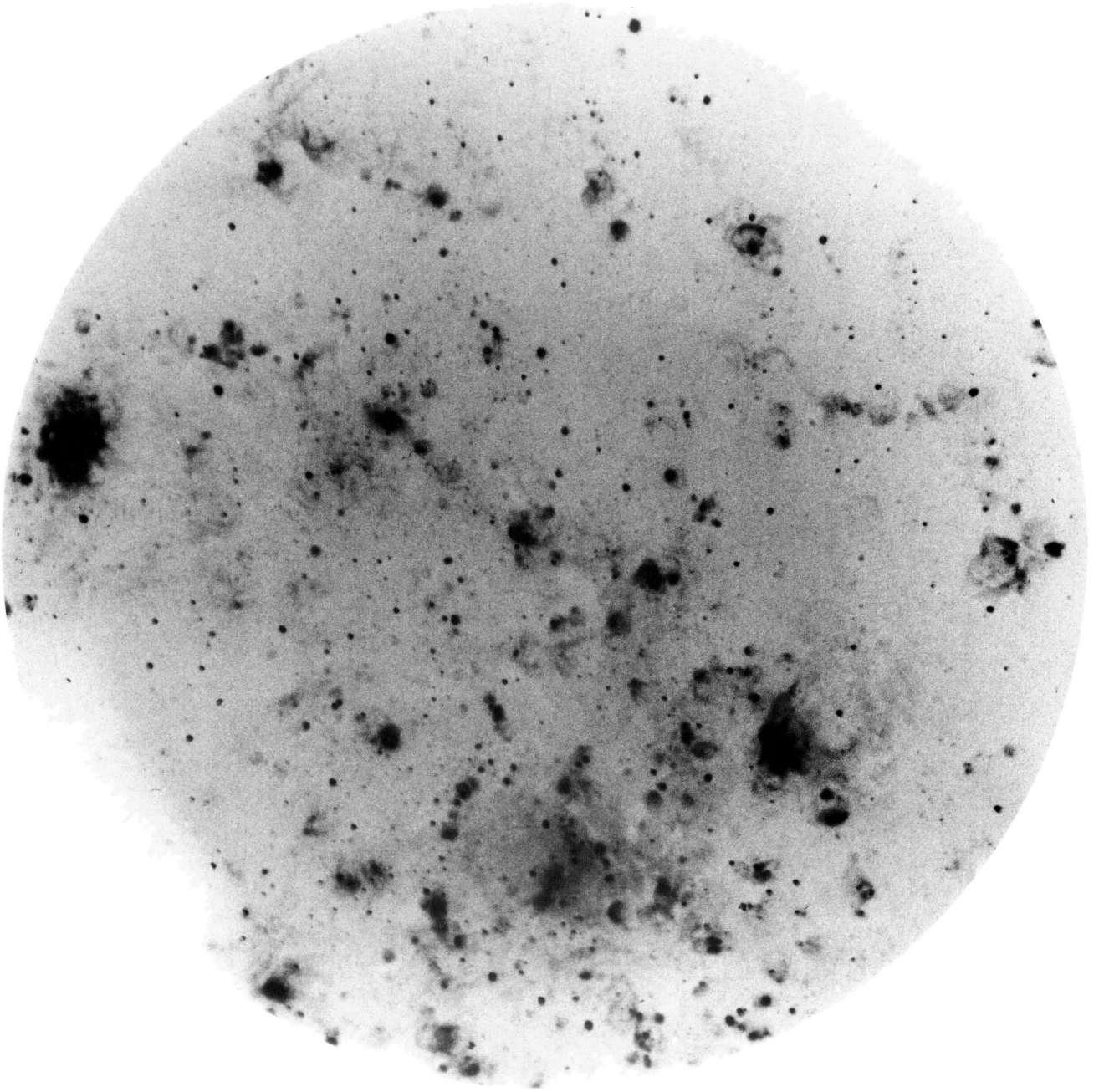

Fig. 6a. Hα photograph of No. 2 (Table 1)

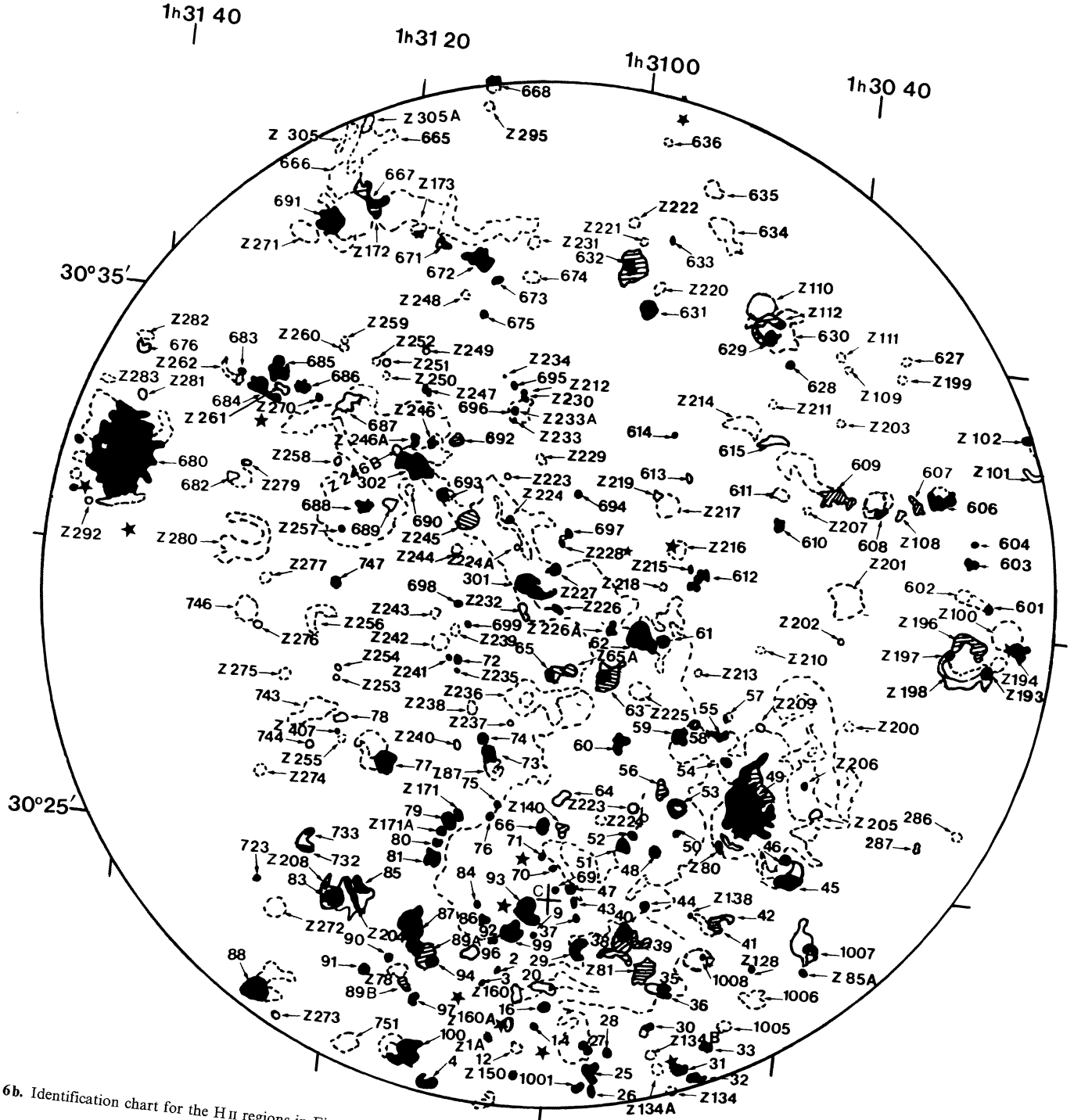

Fig. 6b. Identification chart for the H II regions in Fig. 6a (1950.0 equatorial coordinates)

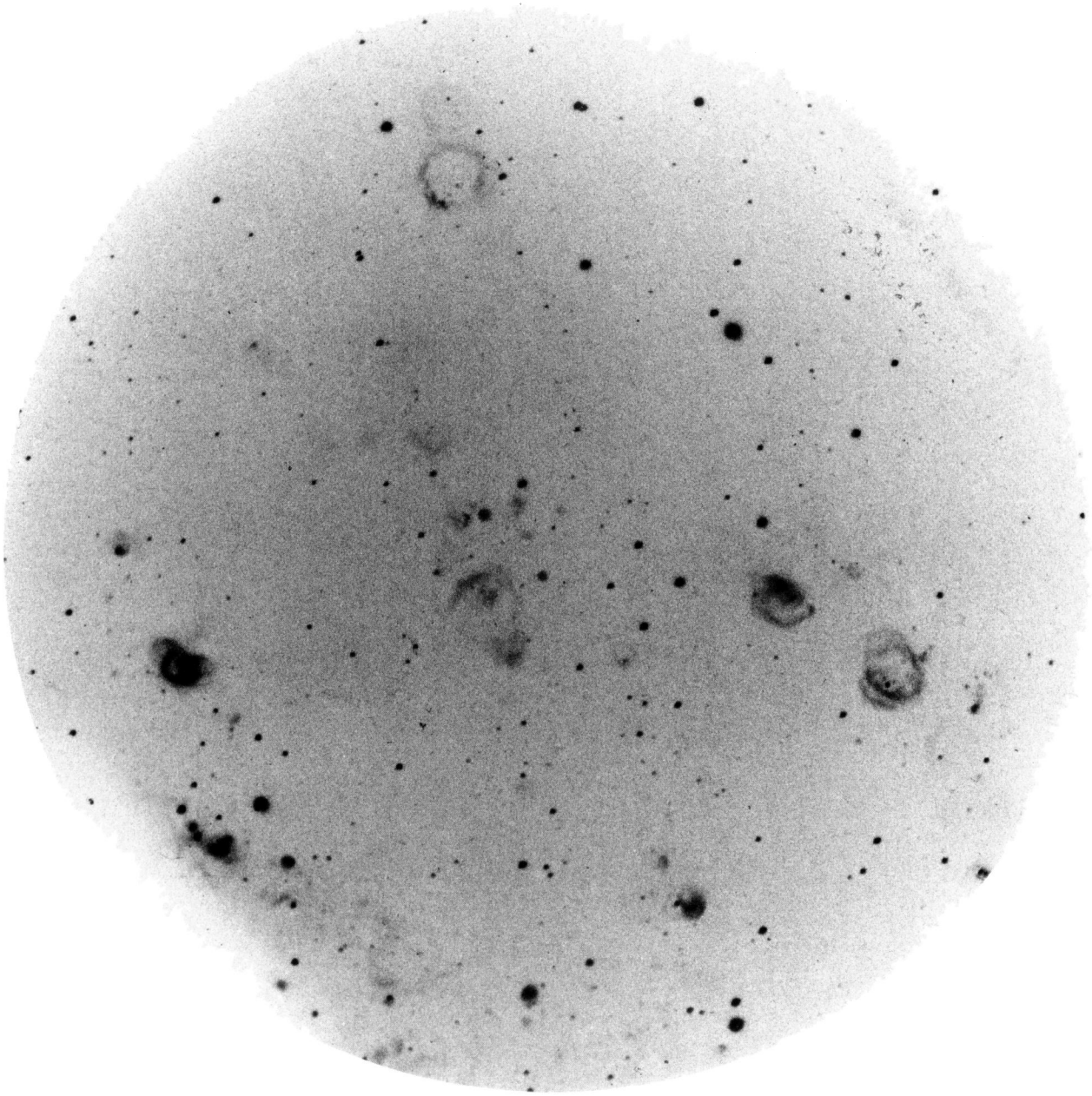

Fig. 7a. Hα photograph of No. 1 (Table 1)

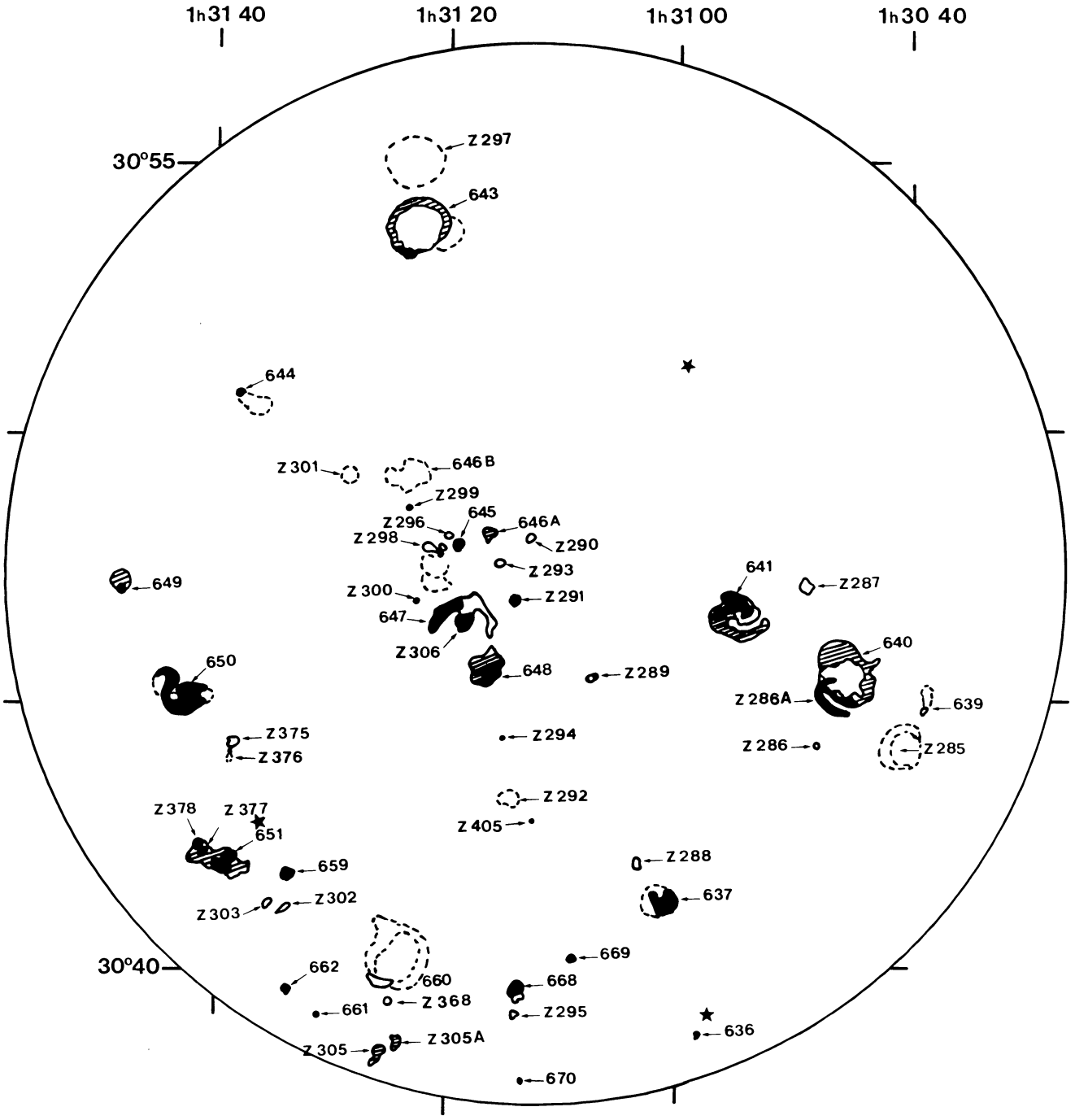

Fig. 7b. Identification chart for the H II regions in Fig. 7a (1950.0 equatorial coordinates)

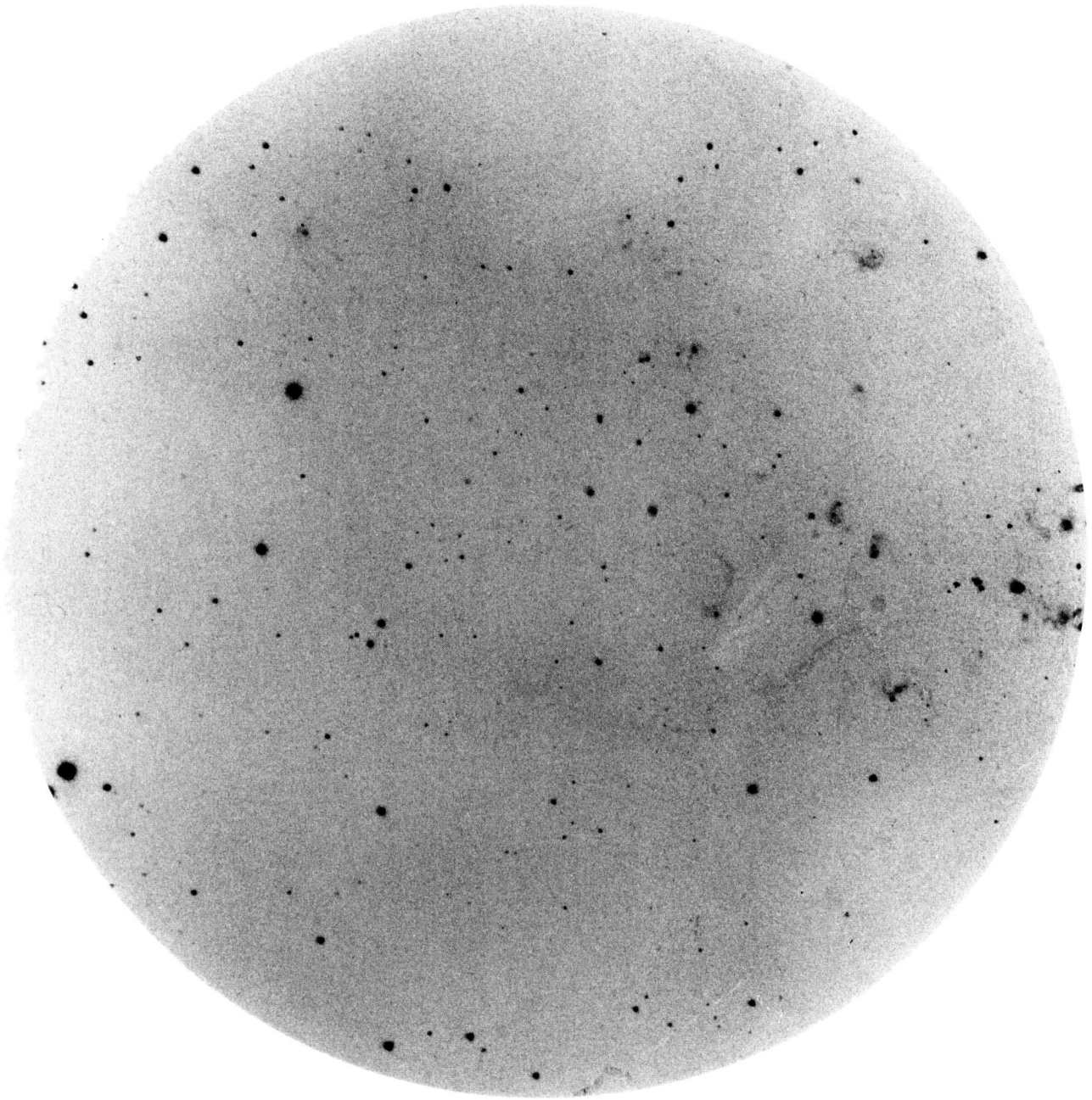

Fig. 8a. Hα photograph of No. 10 (Table 1)

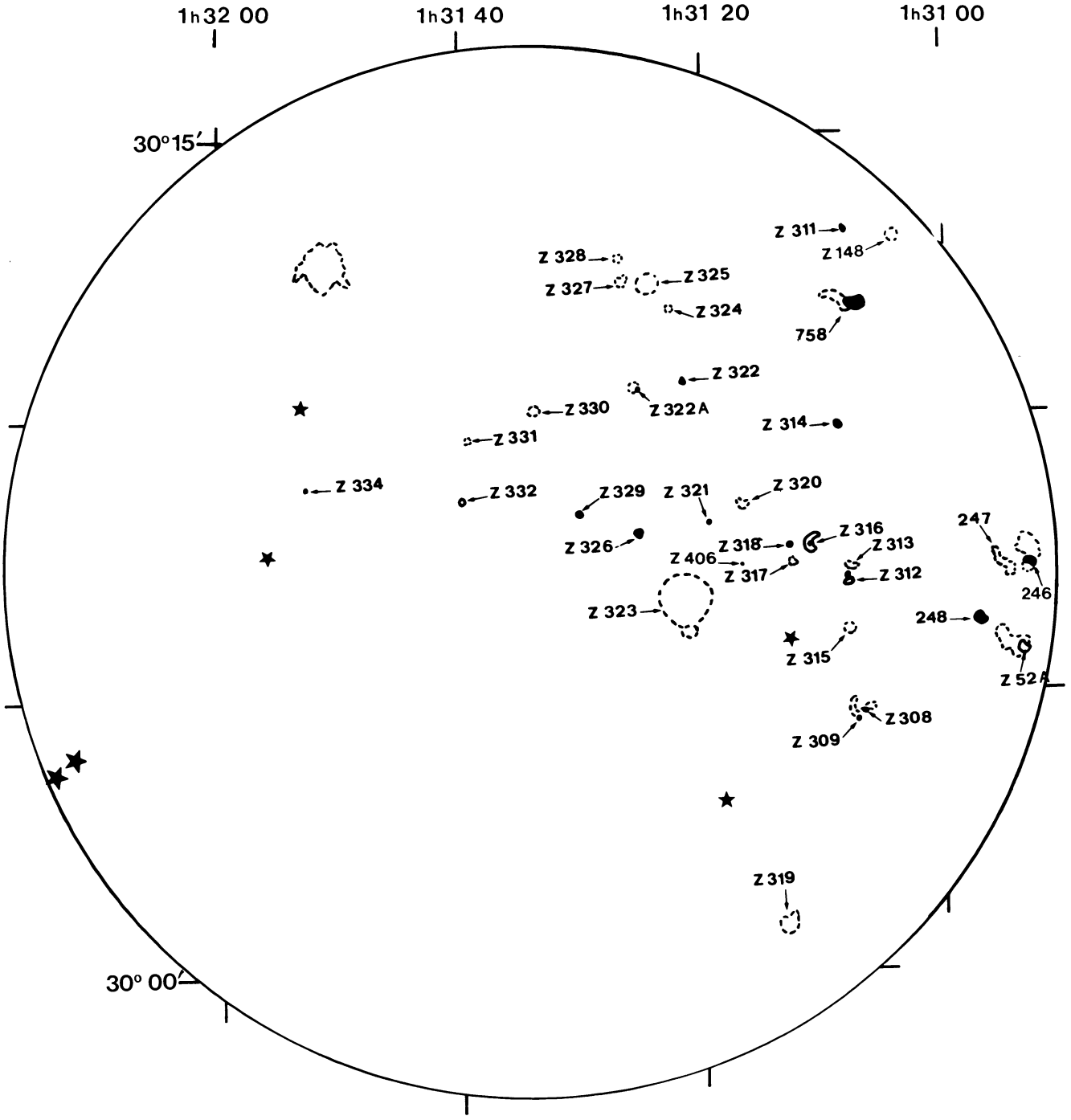

Fig. 8b. Identification chart for the H II regions in Fig. 8a (1950.0 equatorial coordinates)

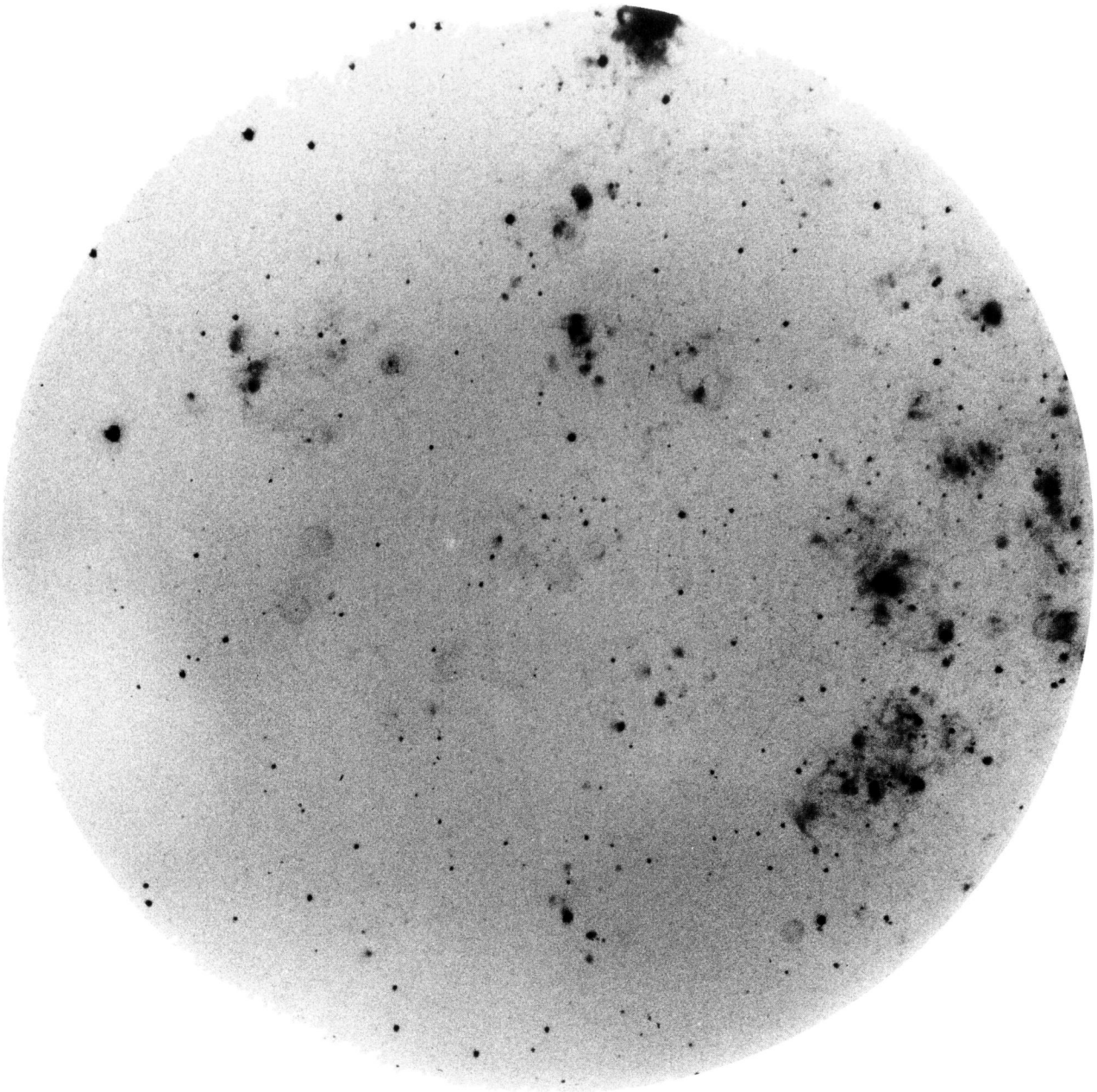

Fig. 9a. Hα photograph of No. 6 (Table 1)

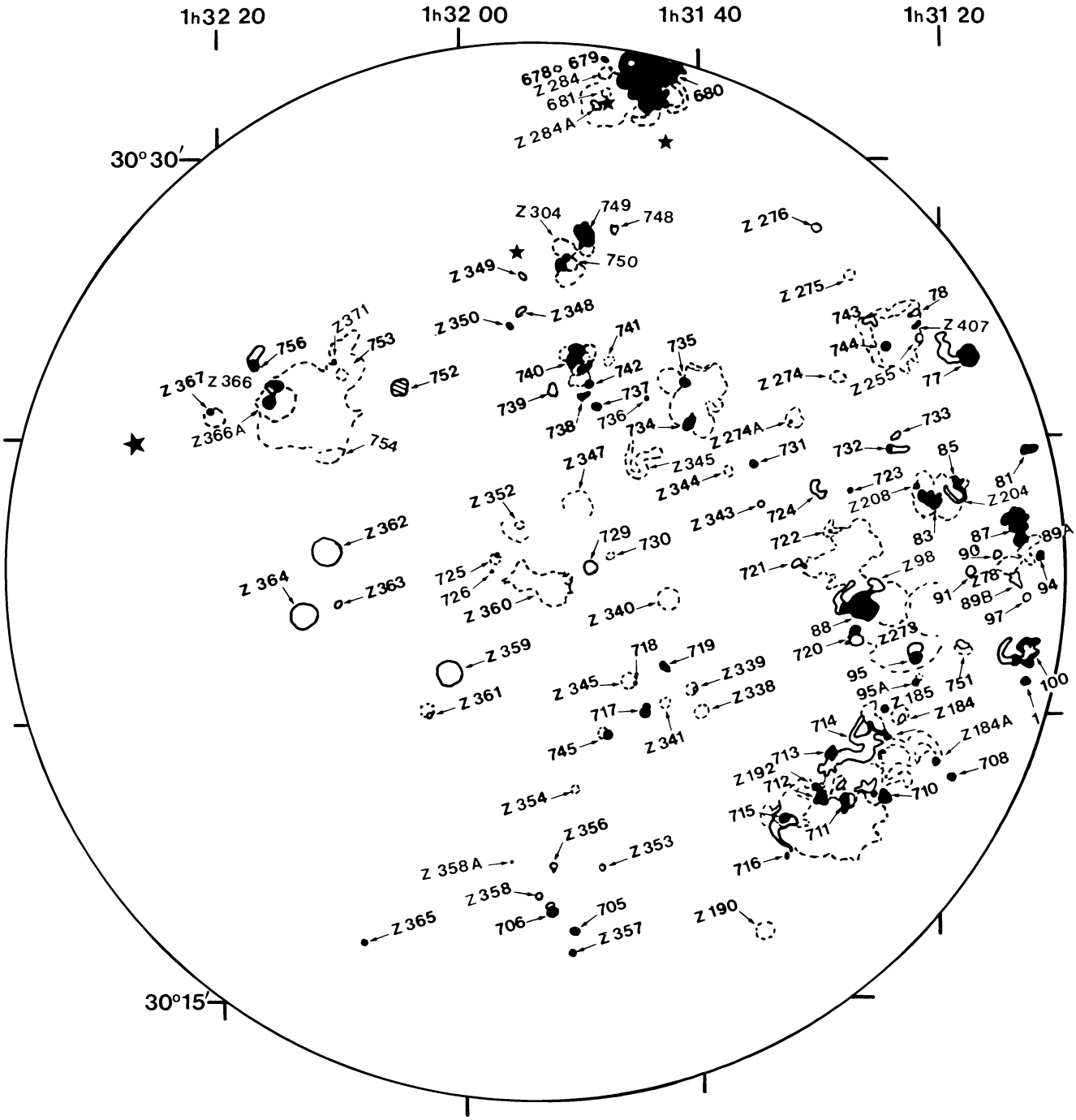

Fig. 9b. Identification chart for the H II regions in Fig. 9a (1950.0 equatorial coordinates)

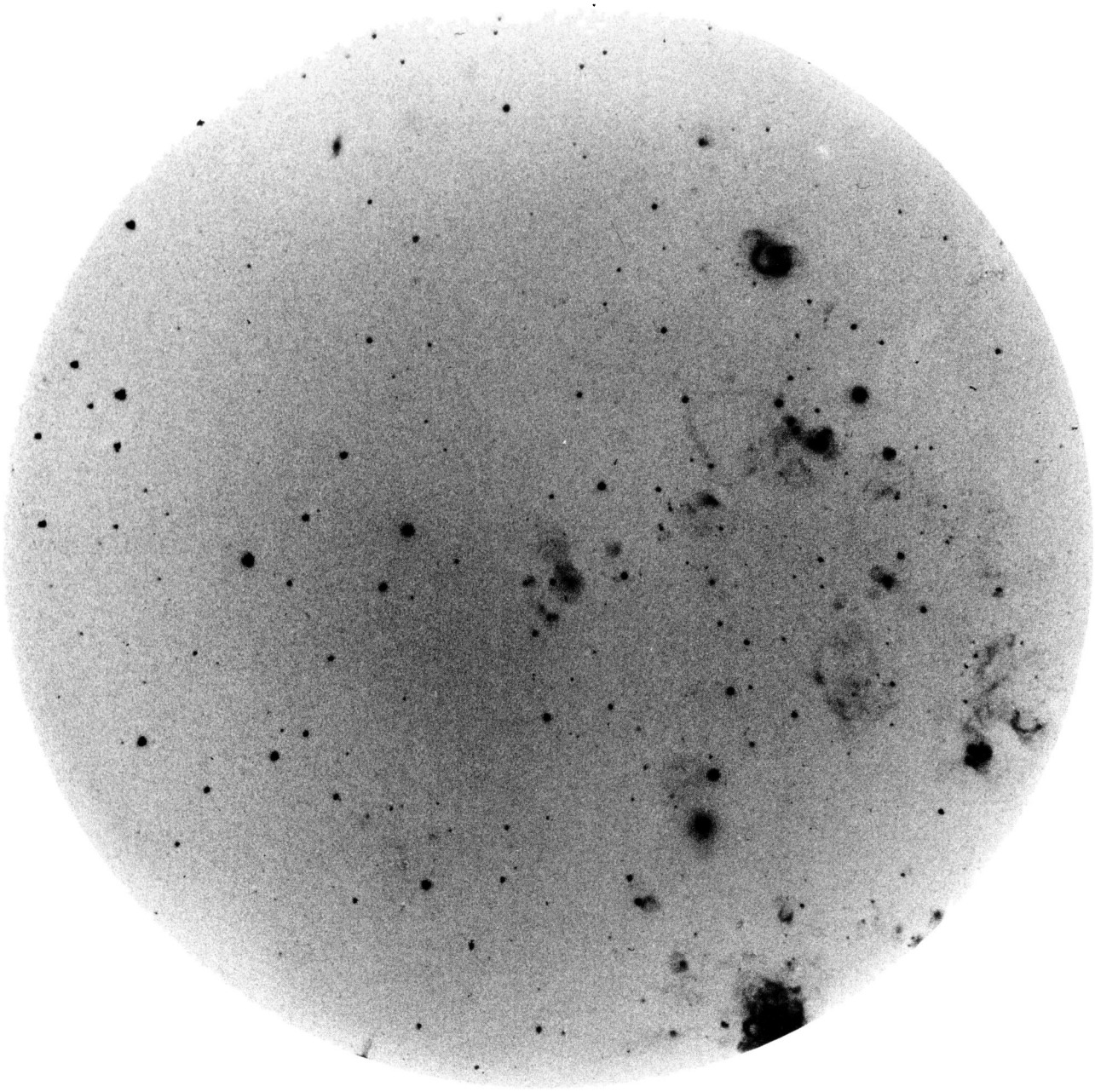

Fig. 10a. Hα photograph of No. 8 (Table 1)

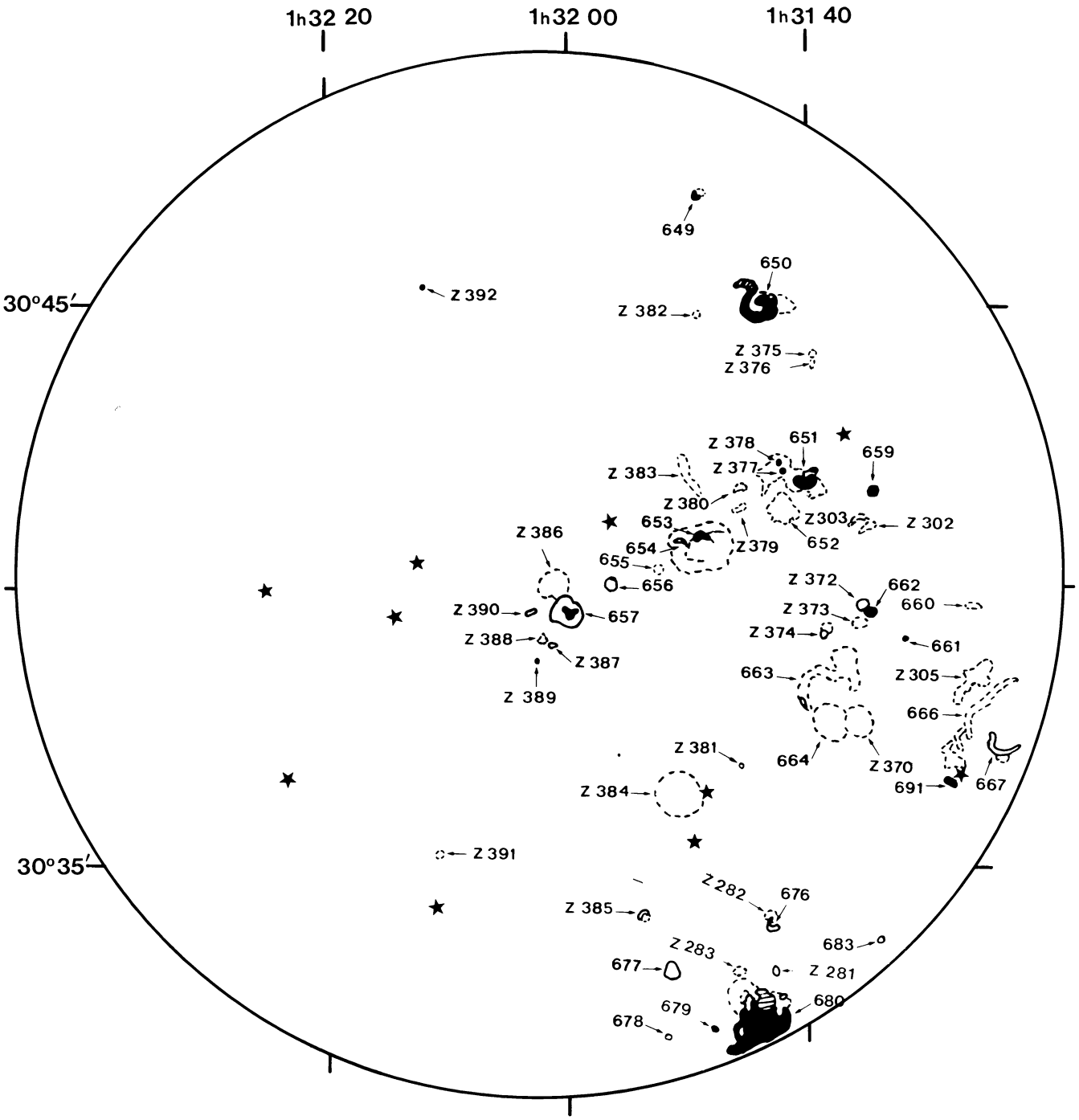

Fig. 10b. Identification chart for the H II regions in Fig. 10a (1950,0 equatorial coordinates)

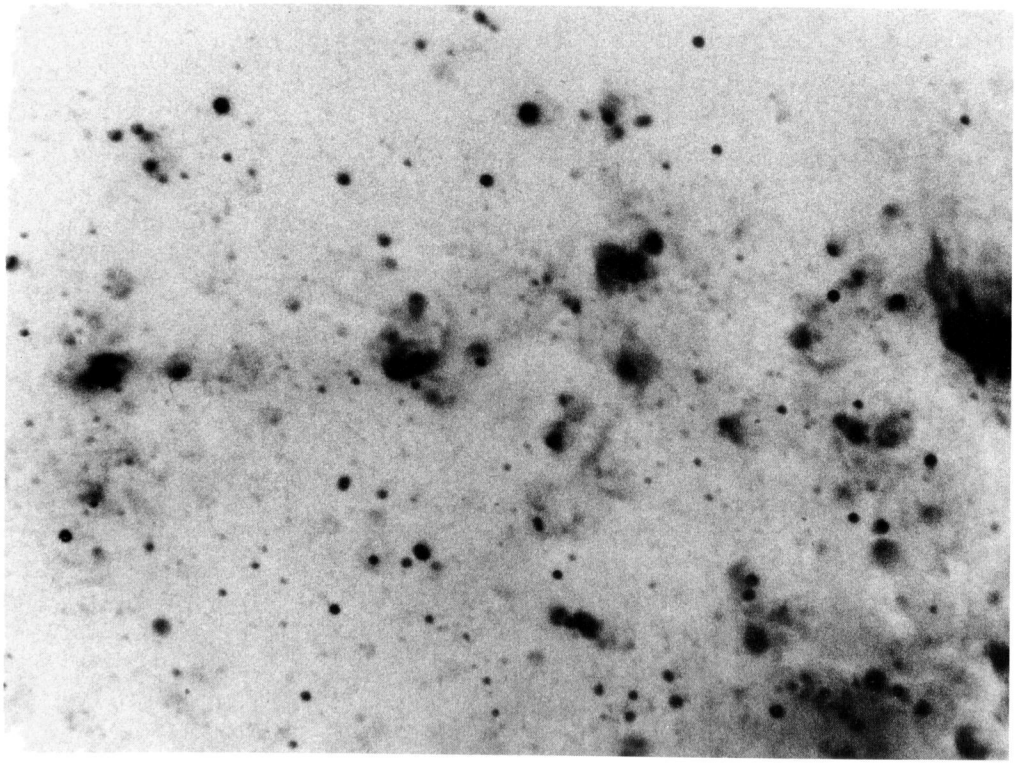

Fig. 11. Enhanced contrast image of a large portion of the northern arm of M33 obtained by superimposing frames 11 and 2 (Fig. 6a). This high contrast print enhances the complex filamentary structure of the Hα background. Note the thin, elongated filaments running parallel to the arm

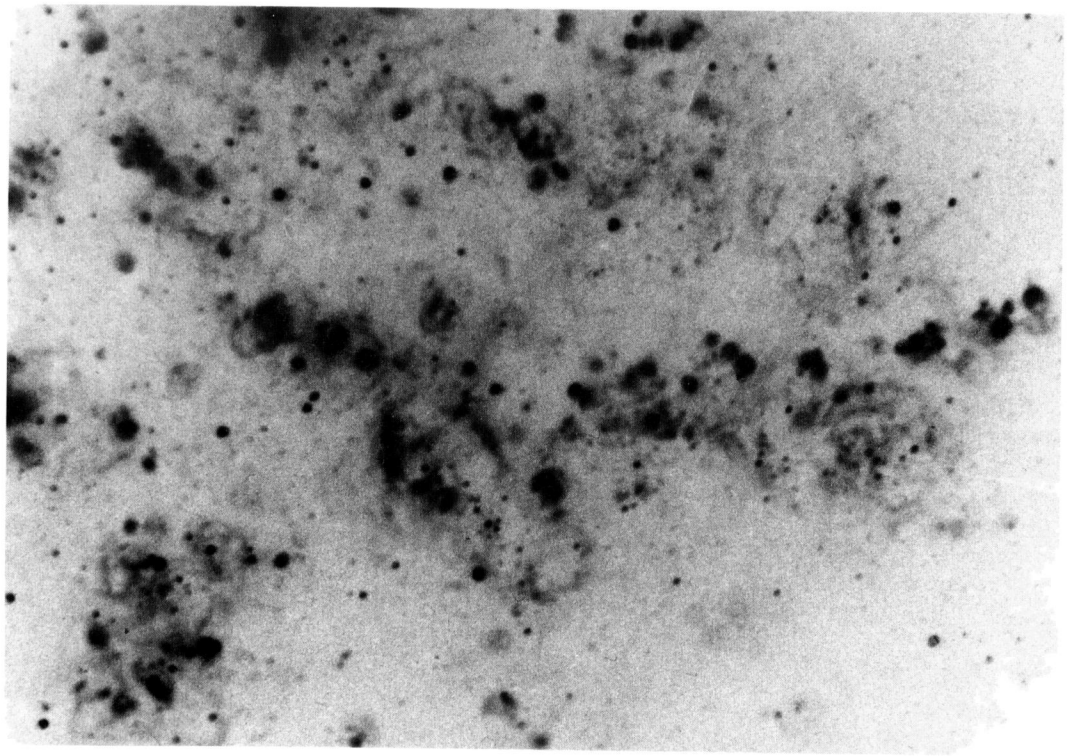

Fig. 12. Amplified image of a large portion of the southern arm of M33 obtained by superimposing frames 11 and 3 (Fig. 5a). The evidence of diffuse interarm emission is revealed by its complex patchy and filamentary structure all over the interarm region. Note the large, circular area including regions 202, 203, 204 and Z 265 (see Figs. 5a and 5b for identification)